Geosciences Faculty Research   Geosciences Department

7-2021

Leveraging Detrital Zircon Geochemistry to Study Deep Arc Processes: REE-Rich Magmas Mobilized by Jurassic Rifting of the Sierra Nevada Arc

D. Clemens-Knott

Kathleen DeGraaff Surpless
Trinity University, ksurples@trinity.edu

A. P. Barth

J. L. Wooden

Leveraging detrital zircon geochemistry to study deep arc processes: REE-rich magmas mobilized by Jurassic rifting of the Sierra Nevada arc

Diane Clemens-Knott [a,*], Kathleen DeGraaff Surpless [b], Andrew P. Barth [c], Joseph L. Wooden [d]

[a] Department of Geological Sciences, California State University–Fullerton, Fullerton, CA 92831, USA
[b] Department of Geosciences, Trinity University, San Antonio, TX 78212, USA
[c] Department of Earth Sciences, Indiana University–Purdue University Indianapolis, Indianapolis, IN 46202, USA
[d] U.S.G.S. retired, USA

ABSTRACT

Anomalous trace element compositions of Middle to Late Jurassic detrital zircon separated from Sierra Nevada forearc and intra-arc strata reveal processes of differentiation occurring within the deep arc lithosphere. REE-Sc-Nb-Ti-Hf-U-Th covariations define three populations of atypically REE-rich grains that we interpret as crystallizing from (1) differentiates produced by olivine+clinopyroxene+plagioclase+garnet±ilmenite fractionation; (2) mixing between mafic arc magmas and partial melts of Proterozoic Mojave province crust; and (3) compositionally transient, low Gd/Yb magmas generated by hornblende resorption during decompression. We interpret a fourth population of Middle Jurassic to Early Cretaceous zircons having REE contents similar to "typical" arc zircon but with atypically high Gd/Yb ratios as having crystallized from partial melts of recycled arc crust and from deep-arc differentiates that evolved down-temperature through hornblende saturation. We hypothesize that latest Jurassic extension ripped open the arc, facilitating upward migration and eruption of geochemically anomalous zircon-bearing magmas. The anomalous compositions relative to "typical" arc zircon imply that these zircons and their host magmas rarely reach the upper arc crust, where eruption and/or erosion would release their zircon cargo to the clastic system. Focusing on the trace element compositions of zircons of syn-extensional age represents a productive new strategy for learning about deep magmatic reservoirs and early differentiation pathways within the thick lithosphere of continental margin arcs.

1. Introduction

The use of trace element contents of magmatic zircon to discriminate between tectonomagmatic environments is well established (Grimes et al., 2007, 2015), and applications to complex magmatic environments are rapidly diversifying (e.g., Carley et al., 2014; Padilla et al., 2016). Surpless, Clemens-Knott, Barth and Gevedon (2019) evaluated the extent to which the trace element geochemistry of detrital zircon from Great Valley forearc strata records the temporal and geochemical variability of magmas in the Mesozoic Sierra Nevada arc. Illustrating the utility of tectonic discrimination diagrams, Surpless et al. (2019) identified a population of Middle Jurassic MOR-type zircon sourced in the Coast Range ophiolite (Colgan & Stanley, 2016; Shervais, Murchey, Kimbrough, Renne & Hanan, 2005), supporting interpretations regarding the timing of accretionary wedge uplift.

Some Great Valley forearc detrital zircons have Sc/Yb similar to the very low ratios typical of ocean island (OI) zircon (Surpless et al., 2019); plume magmatism, however, has never been invoked as a component of Sierra Nevada arc magmatism. Rare, alkalic OI-type basalts have been identified within other arcs, including the Cascades arc to the north and the Trans-Mexico volcanic belt to the south (Bacon et al., 1997; Ferrari, Petrone & Francalanci, 2001; Mullen, Weis, March & Martindale, 2017; Richter & Carmichael, 1992), so these OI-like detrital zircon may record a distinct mantle source. Alternatively, these detrital zircons may instead reveal magmatic processes operative in the deep arc crust.

The low Sc/Yb Middle to Late Jurassic detrital zircon population is particularly abundant in metasedimentary rocks of the Early Cretaceous Goldstein Peak intra-arc basin (Fig. 1; Clemens-Knott, van der Kolk, Sturmer and Saleeby, 2013b), which we now interpret in conjunction with the published forearc dataset. We use additional trace elements to identify detrital zircon sub-populations that differ from the dense cluster of what are presumed to be "typical" arc zircon, and then consider possible magmatic origins for the anomalous populations. We infer that these geochemically anomalous, Middle to Late Jurassic zircons are not part of the typically accessible bedrock and zircon records of Sierra Nevada magmatism because they crystallized from magmas that generally did not rise into the upper crust. In addition to the possibility that Late Jurassic extension facilitated the rise of magmas that more typically stall and differentiate deep in the arc lithosphere, we hypothesize that mineral reactions driven by decompression of hornblende-phyric magmas created transient magmas, the compositions of which are preserved in zircon that crystallized during arc extension.

2. Background

2.1. The Sierra Nevada arc

Though arguably one of the best-characterized continental margin arcs worldwide, studies of Sierra Nevada magmatism are biased towards silicic rocks of the mid- to upper crustal batholith, particu-
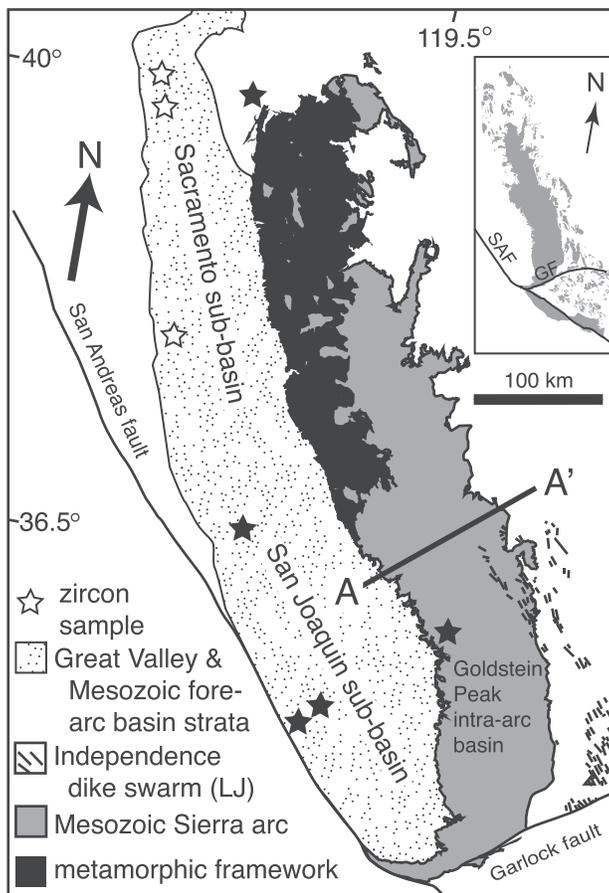

Fig. 1. Generalized geologic map of the Sierra Nevada Mountains and modern Great Valley, California. The Sierra Nevada arc is represented by Mesozoic plutons cut by the northwestern end of the Late Jurassic Independence dike swarm. Deformed Mesozoic marine forearc strata crop out along the western and northern edges of the Great Valley, which is divided into the Sacramento and San Joaquin sub-basins. Stars mark locations of detrital zircon samples (this study and Great Valley sandstones from Surpless et al., 2019); samples containing high-MHREE zircon are marked by black stars. Line A-A' marks the location of a SW-NE conceptual cross-section (Fig. 13) oriented perpendicular to the regional trend of the Independence dike swarm. Inset: igneous rocks (gray pattern) comprising Sierran-Mojave (western half only) arcs; San Andreas (SAF) and Garlock (GF) faults tie the inset to the generalized map.

larly Cretaceous granitoid suites in the glaciated high country (e.g., Bateman, 1992; Coleman & Glazner, 1997; Hirt, 2007; Kistler & Peterman, 1973; Memeti, Paterson, Matzel, Mundil & Okaya, 2010). This record is complemented by rare exposures of mafic plutons (Clemens-Knott & Saleeby, 2013a; James, 1971; Sisson, Grove & Coleman, 1996); peridotite, gabbro and granulite xenoliths carried up from depth by the Miocene diatremes in the west-central foothills (Ducea & Saleeby, 1998a; Chin, Lee, Luffi & Tice, 2012); deep exposures in the southern 'tail' of the Sierra Nevada Mountains (Pickett & Saleeby, 1994); and metamorphosed slices of the arc's volcanic carapace preserved as pendants largely in the central and northern range (Attila, Cottle & Paterson, 2020; Barth, Walker, Wooden, Riggs & Schweickert, 2011, 2012, 2018; Busby-Spera, Mattinson, Riggs & Schermer, 1990).

Midway through the arc's ca. 180-m.y. lifespan, the 600 km-long, basaltic to rhyolitic Independence dike swarm intruded the southeastern to central Sierra Nevada and adjacent ranges (Fig. 1; Chen & Moore, 1979; Glazner, Carl, Coleman, Miller & Bartley, 2008; James, 1989). The northwest-trending Independence dikes tapped magmas from unknown depths in the arc lithosphere and document an abrupt episode of Late Jurassic (148 ± 1 Ma) extension/transtension

oriented subparallel to the axis of the waning Jurassic arc. Evidence of longer-duration Jurassic arc extension is provided by Late Triassic to Middle Jurassic volcanosedimentary pendant sequences that seemingly require an arc-graben system to trap volcano-sedimentary strata within the broad footprint of the Sierra-Mojave arc (Busby, Schermer & Mattinson, 2002; Busby-Spera, 1988).

2.2. The detrital zircon record of arc magmatism

The in situ record of Sierran arc magmatism is augmented by detrital records preserved in arc-proximal basins, which confirm and expand our understanding of arc magmatism. For example, the McCoy Mountains retroarc basin preserves detrital zircon with ages and average trace element compositions that correlate with compositions of plutonic zircon suites for all three magmatic flare-ups of the Sierra-Mojave arc, supporting a connection between arc productivity and magma composition (Barth, Wooden, Jacobson & Probst, 2004, 2013). On the outboard side of the arc, marine sediments deposited in the Great Valley forearc basin preserve both plutonic and volcanic components of the Sierra Nevada arc (e.g., DeGraaff-Surpless, Graham, Wooden & McWilliams, 2002; Ingersoll, 1983; Linn, DePaolo & Ingersoll, 1991; Ojakangas, 1968). Great Valley detrital zircon define a Jurassic age mode shifted towards ca. 148 Ma relative to the ca. 165 Ma Middle Jurassic mode defined by the exposed batholith (Paterson & Ducea, 2015), possibly reflecting arc asymmetry and/or a more representative preservation of the volcanic arc in the detrital record (Surpless et al., 2019). Forearc detrital zircon also define a significant ca. 120 Ma Early Cretaceous age mode that is not well-represented in the exposed batholith, possibly indicating that this westernmost part of the Sierran arc was largely eroded and then buried by eastwardly onlapping forearc sediments.

2.3. Zircon trace element geochemistry

Rare earth elements (REE) are particularly useful in petrology because predictable size-valence relationships control their incorporation into crystallizing phases and thus provide indirect records of mineral substitution. In this study, we use threshold values to define "high" and "intermediate" REE contents relative to what we observe to be low "typical" Sierra Nevada arc zircon values for Ce (a light REE, or LREE); Gd (a medium REE, or MREE); and Yb (a heavy REE, or HREE), the latter two being combined in the acronym MHREE. Selection of these specific REE, instead of those more typically investigated in bulk-rock-based petrogenetic studies (e.g., La, Dy, Lu or Y), was influenced by analytical considerations specific to zircon analysis by SIMS; for example, Ce yields the most precise LREE data from zircon (Coble et al., 2018).

In arc systems, zircon MHREE abundances and REE ratios are strongly influenced by the presence of hornblende and garnet. MHREE are compatible in hornblende crystallizing from intermediate to silicic, calc-alkaline magmas that dominate upper arc crust ($Kd_{hb-melt}$ ca. 1–10; Nandedkar, Hurlimann, Ulmer & Muntener, 2016; Sisson, 1994; Tiepolo, Oberti, Zanetti, Vannucci & Foley, 2007) making it unlikely that most high-MHREE zircon of this study (most of which have Gd > 100 ppm and Yb > 1000 ppm) crystallized from arc magmas that had previously reached hornblende saturation. Furthermore, Yb is extremely compatible in garnet, generating relatively high Gd/Yb ratios in mutually equilibrated phases, including arc magmas fractionating garnet or partial melts of garnetiferous rocks (Grimes, Wooden, Cheadle & John, 2015). High Gd/Yb ratios in arc magmas are typically associated with high melting and/or crystallization pressures because magmatic garnet is estimated to crystallize in arc magmas at pressures greater than ca. 1 GPa (Ulmer, Kaefi & Muntener, 2018) and in hydrous mantle peridotite at pressures above 1.6 GPa (Gaetani & Grove, 1998). Metamorphic garnet, however, is stable at pressures as low as ca. 0.35 GPa in the Sierran arc crust (e.g., Chin, Lee & Tollstrup, 2013; Strickland et al., 2013), complicating pressure estimates for partial melts of the metamorphic framework and any zircon that crystallized from them.

Interpretation of zircon Gd/Yb ratios is further complicated by the temperature-dependent variation of zircon-magma distribution coefficients (Claiborne et al., 2018), as well as by the generally higher compatibility of Yb relative to Gd in zircon, which decreases the high Gd/Yb ratios predicted for magmas in equilibrium with garnet. Therefore, although quantitative (i.e., pressure) interpretations of zircon Gd/Yb ratios are impossible, high Gd/Yb ratios in arc-derived detrital zircon likely point to equilibrium between magmas and either metamorphic or magmatic garnet at mid-crustal to mantle depths.

Additional trace elements central to interpretation of melt composition and zircon crystallization histories (Grimes et al., 2015) include the high field strength elements Hf, Th and U, which are highly compatible in zircon, and the transition metal *Sc*, which is variably compatible in many igneous ferromagnesium silicates (e.g., garnet, clinopyroxene, amphibole). We use titanium for its relative record of temperature (i.e., zircon with high Ti concentrations crystallized at relatively high temperature), although we do not calculate temperatures using the Ti-in-zircon thermometer due to the unknown chemistry of melts from which these detrital zircons crystallized (i.e., SiO_2 and TiO_2 activities; Ferry & Watson, 2007). Lastly, niobium (Nb) concentration is important for zircon-based tectonic discrimination diagrams (Grimes et al., 2015) and low Nb relative to other moderately incompatible elements is recognized as a global geochemical signal of arc magmatism (Barth et al., 2017a; 2018).

Grimes et al. (2015) emphasize the interpretation of trace element ratios in order to neutralize the large ranges in absolute element concentrations observed within zircon suites that result from changes in distribution coefficients caused by varying crystallization temperatures. We use both trace element ratios and absolute concentrations because ratios may mask variations in trace element concentrations that potentially indicate the operation of specific magmatic processes.

3. Samples and methods

We combine trace element data of selected grains from three previously dated detrital zircon samples from the Goldstein Peak intra-arc basin ($n = 83$; Fig. 1; ST-A; Clemens-Knott, van derKolk, Sturmer, Saleeby, 2013b) with data from seven samples of the Great Valley Group marine strata collected along the length of the Great Valley forearc basin ($n = 246$; ST-C; Fig. 1). We exclude the subset of MOR-type detrital zircon from the forearc basin that Surpless et al. (2019) argued were sourced in the Coast Range ophiolite. The Goldstein Peak samples are weakly metamorphosed, Berriasian to Valanginian fluvial sediments (ca. 140–135 Ma; Martin & Clemens-Knott, 2015), and the Great Valley Group samples are unmetamorphosed Tithonian to Campanian marine strata (ca. 152 – 72 Ma; DeGraaff-Surpless et al., 2002; Orme & Surpless, 2019). Similar detrital zircon U-Pb age distributions indicate shared arc provenance for Goldstein Peak and forearc strata, suggesting that Early Cretaceous fluvial systems linked the Goldstein Peak intra-arc with forearc depositional systems (Clemens-Knott et al., 2013b; Martin & Clemens-Knott, 2015).

Trace-element concentrations (DR1) were measured by sensitive high-resolution ion microprobe–reverse geometry (SHRIMP-RG) methods (Barth & Wooden, 2010; Grimes et al., 2015; Mazdab & Wooden;, 2006). Ti values were recalculated based on results of Coble et al. (2018); all other concentrations are calibrated to the original Madagascar green (MAD) zircon standard (Barth & Wooden, 2010). Based on repeat analyses of MAD standards, 1σ errors for REE reported in this study range from 1.7% (Eu) to 5.9% (Ce), with slightly higher errors for Sc (7.1%) and Nb (9.0%) due to mass resolution issues (Barth & Wooden, 2010; Coble et al., 2018). Due to its high mass resolution capabilities relative to other instruments, the SHRIMP-RG is well suited for relatively precise analysis of Nb and Sc abundances; Nb and Sc compositions are key characteristics of many high-MHREE zircon making instrumentation selection important for our analytical strategy. We used cathodoluminescence or backscattered electron images to guide anal-
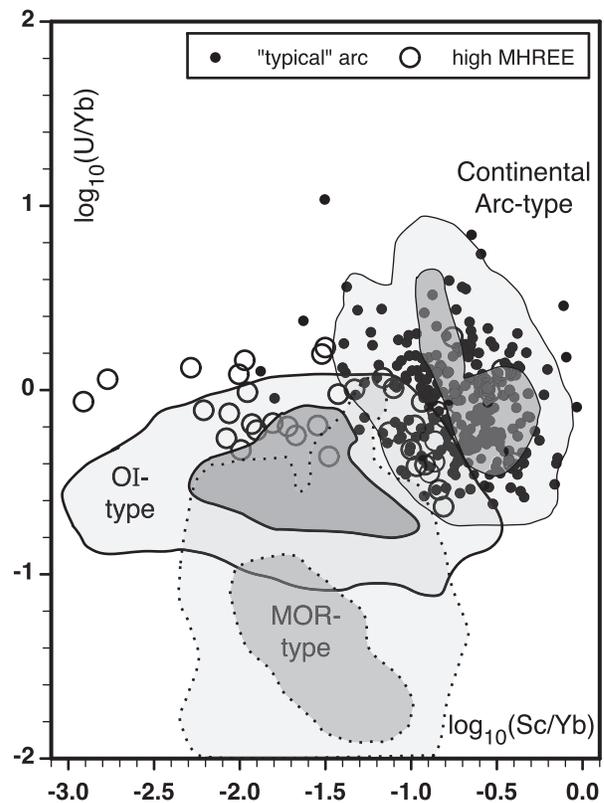

Fig. 2. Detrital zircon compositions plotted on a $\log_{10}(Sc/Yb)$ vs. $\log_{10}(U/Yb)$ tectonic discrimination diagram: contours at 50% (dark gray fill) and 95% (light gray fill) are shown for continental arc, ocean island (OI), and mid-ocean ridge (MOR) type zircon (after Grimes et al., 2015). Continental arc contours based on the Peninsular Ranges and Cascades arcs and the Taupo volcanic field (Barker et al., 2014; Barth & Wooden, 2010; Carley et al., 2014; Chamberlain, Wilson, Wooden, Cherlier & Ireland, 2014; Claiborne, 2011; Wooden, unpublished data). High-MHREE zircon have both Gd > 50 ppm (most exceed 100 ppm) and Yb > 535 ppm (most exceed 1000 ppm). Small black circles identify grains with lower concentrations of medium-heavy REE (MHREE), which appear to represent the "typical" background values for this arc. Sample locations, U-Pb isotopic data, and trace element data are tabulated in ST-A.

ysis of previously dated grains, placing trace-element pits as close to filled U-Pb pits as the clastic grain morphology permitted. We verified prior LA-ICP-MS age determinations by monitoring $^{206}Pb/^{238}U$ during trace-element data collection, and we do not include data from zircons with age discrepancies exceeding 5% or with any chemical evidence of inclusions (e.g., Fe > 100 ppm; Grimes et al., 2015). U-Pb ages were calibrated to the R33 zircon standard (419 Ma; Black et al., 2004). REE compositions of host melts were calculated using empirical temperature-dependent correlations of partition coefficients based on titanium concentrations (ST-C; Claiborne et al., 2018), and the effects of decreases in magmatic Ti contents due to ilmenite fractionation prior to zircon crystallization are considered. Ce is not included in host melt REE calculations due to unconstrained redox conditions during crystallization of detrital zircon, which are separated from their plutonic hosts.

4. Results

On the data-contoured $\log_{10}(Sc/Yb) - \log_{10}(U/Yb)$ tectonic discrimination diagram of Grimes et al. (2015), most detrital zircons plot within the continental arc field, as would be expected for these forearc and intra-arc detrital grains (Fig. 2). However, nearly 10% of the 329 detrital zircons plot in, or parallel to, the ocean island (OI) field seemingly implicating a tectonomagmatic regime that has no independent geologic support from past studies of the Sierra Nevada arc.

D. Clemens-Knott, K.D. Surpless, A.P. Barth et al.

The low Sc/Yb of these OI-like grains (i.e., $\log_{10}(Sc/Yb) < -1.0$; Fig. 2) derives in large part from elevated Yb contents (> 535 ppm) relative to "typical" continental arc-type zircon. Although a few OI-like zircons have elevated Ce concentrations (Fig. 3a), the REE anomaly is dominated by the MHREE (i.e., Gd, Yb; Fig. 3bc). High-MHREE zircon as defined for this investigation have both Gd > 50 ppm (most exceed 100 ppm) and Yb > 535 ppm (most exceed 1000 ppm). In addition to elevated Yb contents, half of the high-MHREE zircon have Sc < 10 ppm (DR1), which is unusual for arc zircon (e.g., Sc > 30 ppm for "typical" arc zircon) and further contributes to the observed low Sc/Yb ratios (Grimes et al., 2015). The anomalous MHREE signal is largely restricted to Middle to Late Jurassic grains (Fig. 3).

The majority of the Late Jurassic high-MHREE grains have Nb contents greatly exceeding those of both older and younger "typical" Nb-poor Sierra arc zircon (< 5–10 ppm; Fig. 3d). Globally, arc magmas are distinguished from other tectonomagmatic provinces by a negative niobium anomaly (e.g., lower normalized Nb abundance relative to Th and La), and true plume zircons have high Nb contents (Grimes et al., 2015). The ca. ten-fold increase in Nb concentrations recorded by Late Jurassic high-MHREE zircons may indicate a plume component, or that Nb behaved incompatibly during one or more fractionation processes active in the deep arc lithosphere during the Middle to Late Jurassic.

32 of 35 high-MHREE grains come from the San Joaquin forearc sub-basin and the fluvial-lacustrine protoliths of the Goldstein Peak metamorphic pendant (Fig. 1). Approximately 20% of analyzed zircon from the Goldstein Peak intra-arc basin are high-MHREE grains, reinforcing the spatial connection between this geochemically anomalous zircon population and the southern Sierra Nevada arc.

4.1. Trace element characterization of zircon populations I-IV

We divide high-MHREE zircons into three groups based on Sc/Yb ratios (Fig. 4a): group I extends the trend of relatively REE-poor, "typical" arc zircon to lower Sc/Yb values due to both low Sc and high Yb values; group II has variably elevated Yb concentrations and arc-like Sc/Yb ratios; and group III plots between groups I and II on these axes and is further distinguished from "typical" Sierra arc zircon by its Yb enrichment (Fig. 4b). In addition, unusually high Gd_N/Yb_N ratios (>0.08) in relatively REE-poor zircon identify a fourth zircon group (Fig. 4b). 86% of group IV detrital zircons were separated from San Joaquin Valley forearc samples ($n = 25$) and Goldstein Peak intra-arc basin samples ($n = 7$), with the remainder from Sacramento forearc basin samples ($n = 5$), suggesting the low REE, high Gd/Yb grains of group IV were also sourced predominantly in the southern Sierra Nevada arc.
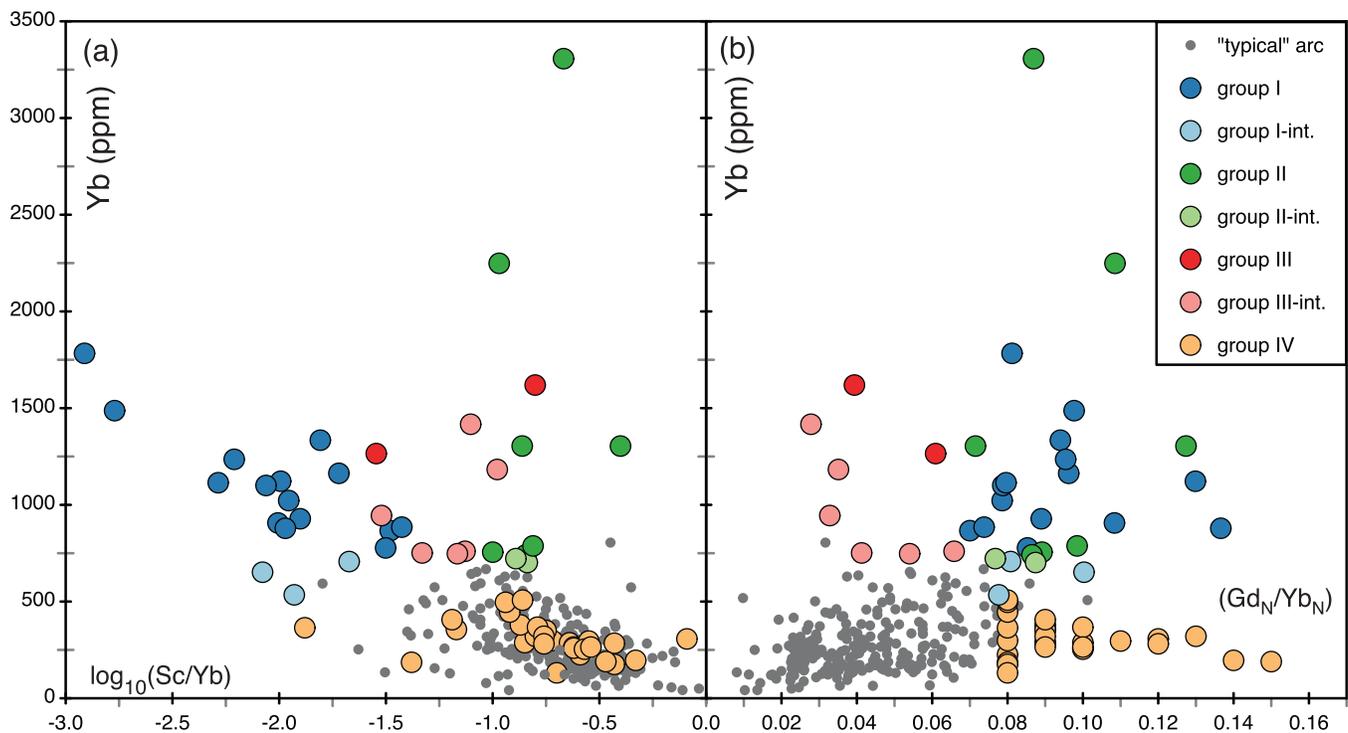
In Fig. 5 we compare detrital zircon from the Sierra Nevada arc to data from the Cascades arc (including Mt. St. Helens), the Izu-Bonin island arc, and the Northern Volcanic Zone of the Andean arc (Barth et al., 2017a; Claiborne, 2011; Dilles et al., 2015). Overlap between the dense cluster of published arc data (gray crosses) and that of "typical" detrital zircon from the Sierra Nevada arc (gray dots) provides a global context for our use of "typical" to describe the dominant population of relatively REE-poor detrital zircon. These modern arcs contain high-MHREE igneous arc zircon similar to detrital groups II and III but virtually none are similar to the low-Sc/Yb zircon of group I. Covariations between Gd/Yb and Sc/Yb provide the clearest geochemical demarcation between high-MHREE groups I, II and III (Fig. 5b).

4.2. U-Pb geochronology

Previously published LA-ICP-MS U-Pb ages of high-MHREE forearc and intra-arc detrital zircon are presented by geochemical group (Fig. 6; ST-A). Sixteen of 18 zircon comprising high-MHREE group I crystallized at the end of the Late Jurassic (ca. 150 Ma), as did three of the nine group II zircon. Seven of 8 group III zircon are Middle to Late Jurassic in age. Relatively REE-poor group IV zircons range in age from Early Jurassic to early Late Cretaceous. None of the high-MHREE zircon are Triassic;
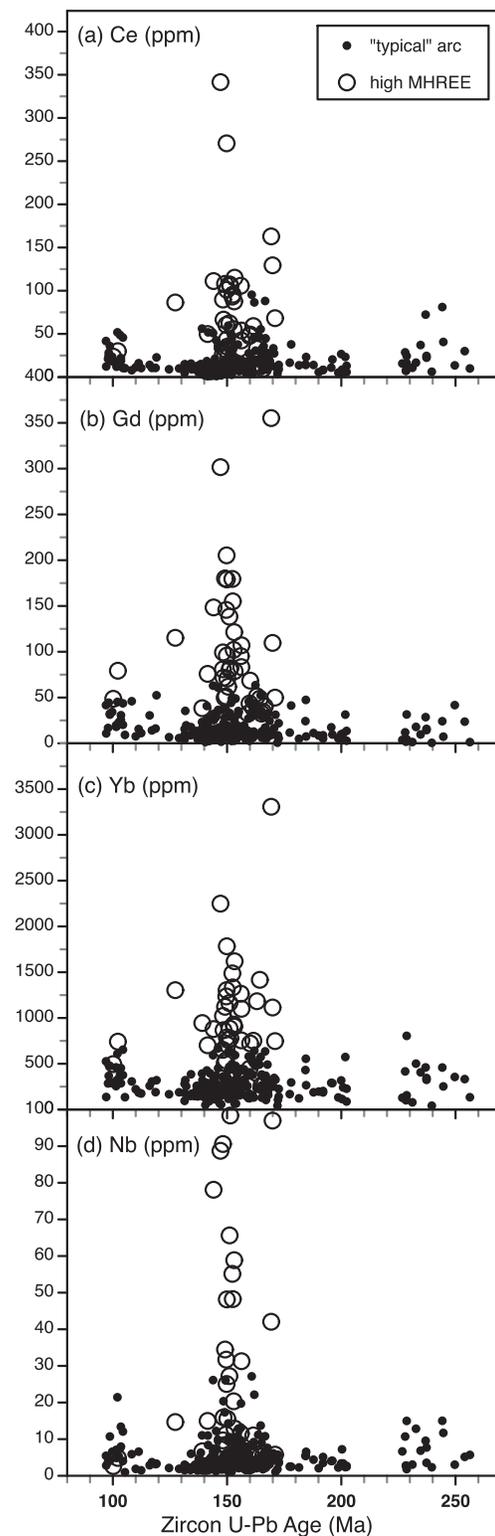
Fig. 3. Concentrations (ppm) of representative (a) light (Ce), (b) medium (Gd), and (c) heavy (Yb) REE; and (d) niobium concentrations in detrital arc zircon through the Mesozoic. Symbols as in Fig. 2. In this and following figures, symbol size exceeds $\pm 1\sigma$ error.

ARTICLE IN PRESS

JID: RINGEO [m5GeSdc;August 10, 2021;13:6]

D. Clemens-Knott, K.D. Surpless, A.P. Barth et al. Results in Geochemistry xxx (xxxx) xxx

Fig. 4. Variations of Yb relative to (a) $\log_{10}(Sc/Yb)$, which divides high-MHREE grains into group I (blue), group II (green) and group III (red) relative to "typical" arc zircon. Dark shades identify group I-III zircon containing more than 70 ppm Gd and 740 ppm Yb; light shades identify group I-III zircon having intermediate MHREE concentrations ("int."), specifically 70 > Gd > 50 ppm, 740 > Yb > 535 ppm, as well as log Sc/Yb < −1.5 (Fig. 2). Intermediate group III (pink) is expanded to include four Yb-rich zircon having Gd between 38 and 50 ppm (see text); and (b) $\log_{10}(Gd_N/Yb_N)$ vs. Yb which shows the high Gd_N/Yb_N of group I and II zircon, implicating crystallization from magmas in equilibrium with garnet. Group IV (orange) are "typical" low-REE arc zircon having Gd_N/Yb_N values (>0.08) as high as groups I and II. Normalized MHREE values are used to facilitate comparison to published REE spidergraphs. (For interpretation of the references to color in this figure legend, the reader is referred to the web version of this article.).

this may in part be an artifact of the small number of Triassic detrital zircons found in the forearc basin (Surpless et al., 2019).

5. Interpretation

The dominantly Late Jurassic ages of high-MHREE detrital zircon suggest a connection to the ca. 150 Ma extensional/transtensional event that facilitated emplacement of the Independence dike swarm for 600 km along the Jurassic Sierra-Mojave arc axis (Carl & Glazner, 2002; Glazner, Bartley & Carl, 1999). Although the magnitude of Mesozoic crustal extension in the Sierra-Mojave arc is debated (e.g., Barth et al., 2017b; Cao et al., 2015; Dunne & Walker, 2004; Schermer, Busby & Mattinson, 2002; Walker, Martin & Glazner, 2002), Late Jurassic crustal extension could have enabled the rise of magmas formed in the arc root that would otherwise have been trapped and crystallized in situ in a neutral to compressional tectonic regime.

In the following sections, we evaluate the hypothesis that the predominantly Late Jurassic, anomalously REE-rich detrital zircon preserved in the Sierra Nevada forearc and intra-arc basins are geochemically unlike "typical" arc zircon that are sourced in the felsic volcano-plutonic arc mass because they crystallized from mafic arc magmas that seldom escape the deep arc crust (e.g., Sisson et al., 1996). To interpret the anomalous zircon trace element data, we consider magmatic processes that are typically invoked for the earliest, deepest stages of magmatic differentiation within continental margin arcs: high-temperature fractional crystallization of mantle-derived basaltic magmas; partial melting and assimilation of metavolcanosedimentary lower continental crust by mantle-derived magmas; and recycling of arc lithosphere, including arclogites, by partial melting. In addition, we consider crystal resorption reactions that occur during extension-aided upwelling and decompression of deep-seated magmas. We identify specific differen-

tiation processes capable of producing seemingly anomalous magmas within the deep arc crust from which the observed high-MHREE zircon might have crystallized. In doing so, we assume that each geochemical group is composed of detrital zircon originally crystallized from separate magma bodies that had evolved to varying extents along similar differentiation pathways.

5.1. Fractional crystallization (group I zircon)

Olivine, pyroxene, hornblende and plagioclase feldspar are the rock-forming silicate minerals most likely to crystallize from mafic to intermediate magmas in the mid- to deep arc crust, with igneous garnet a possibility deep in the overthickened roots of long-lived continental margin arcs. REE are strongly compatible in amphibole, making it unlikely that significant hornblende fractionation occurred prior to crystallization of groups I-III MHREE-rich zircon. Furthermore, the Sc/Yb 〈 0.04 that characterizes group I zircon is significantly below zircon Sc/Yb ratios 〉 0.1 that typically form in the presence of fractionating amphibole (Grimes et al., 2015).

REE are strongly incompatible in olivine, and incompatible to weakly compatible in the pyroxenes, making these mafic phases potential suspects in the creation of REE-rich magmas by fractional crystallization. Enrichment of all REE and Sc due to significant olivine fractionation is petrologically reasonable but cannot be directly assessed using zircon because zircon does not preserve any unique trace element signals of olivine fractionation. Pyroxene is the only rock-forming silicate mineral that can deplete a magma in Sc without simultaneously depleting the magma in REE. Both clino- and orthopyroxene are possible fractionating phases in arc magmas; empirical and experimental data indicate that clinopyroxene is generally more abundant than orthopyroxene in mid-
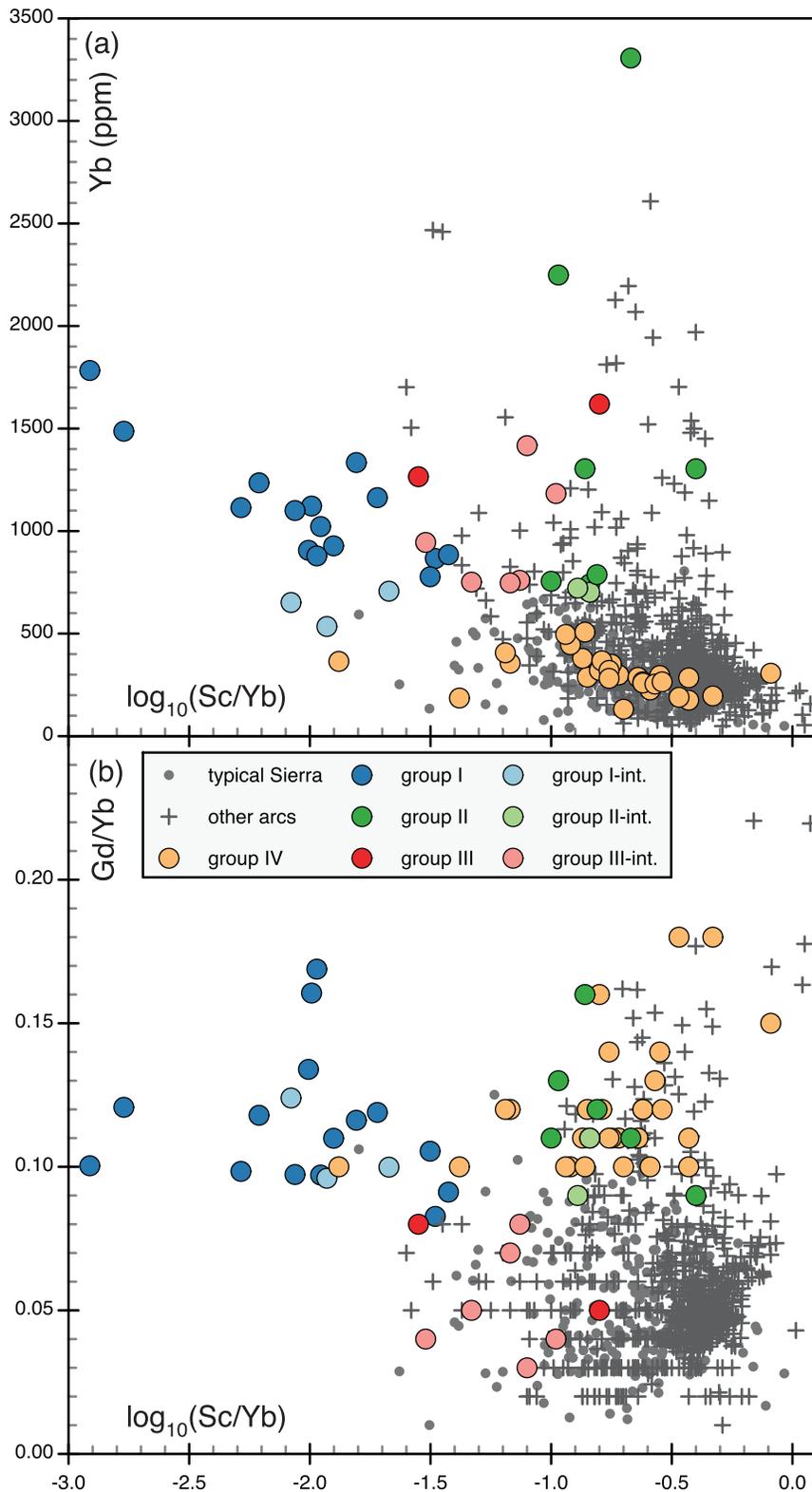
Fig. 5. Variations relative to $\log_{10}(Sc/Yb)$ of (a) Yb, and (b) Gd/Yb (not chondrite normalized, to facilitate comparisons of raw data). Fig. 5a differs from Fig. 4a by the addition of published arc data from the Andes, Cascades and Izu-Bonin arcs (crosses; $n = 682$). Two zircons with extremely high Gd/Yb (0.5, 0.65) are omitted. Fig. 5b is a combination of axes from Fig. 4ab, which emphasizes the clear divisions between high-MHREE zircon of group I (low Sc/Yb; high Gd/Yb), group II ("typical" arc Sc/Yb; high Gd/Yb), and group III ("typical" arc Sc/Yb; low Gd/Yb). Published arc data from Claiborne (2011), Dilles et al. (2015), and Barth et al. (2017a). (For interpretation of the references to color in this figure legend, the reader is referred to the web version of this article.)

to deep arc crust (e.g., Lee, Cheng & Horodyskyj, 2006; Ulmer et al., 2018).

With the exception of Eu^{+2}, REE are extremely incompatible in plagioclase feldspar, making plagioclase fractionation a particularly efficient mechanism for generating REE-rich magmas while simultaneously generating a hallmark negative europium anomaly (Eu/Eu*). Any negative magmatic Eu/Eu* produced in the melt will be preserved in any

zircon that subsequently crystallize, magnifying the slight relative incompatibility of Eu^{+2} relative to Sm^{+3} and Gd^{+3} inherent to zircon (Bea, Pereira & Stroh, 1994). Virtually all of the detrital zircons in this study display negative europium anomalies (i.e., Eu/Eu* = 1 to 0.1; Fig 7a); high-MHREE group I zircon, however, are characterized by unusually large negative Eu anomalies (i.e., Eu/Eu* < 0.1) indicating significant plagioclase fractionation prior to zircon crystallization. Group
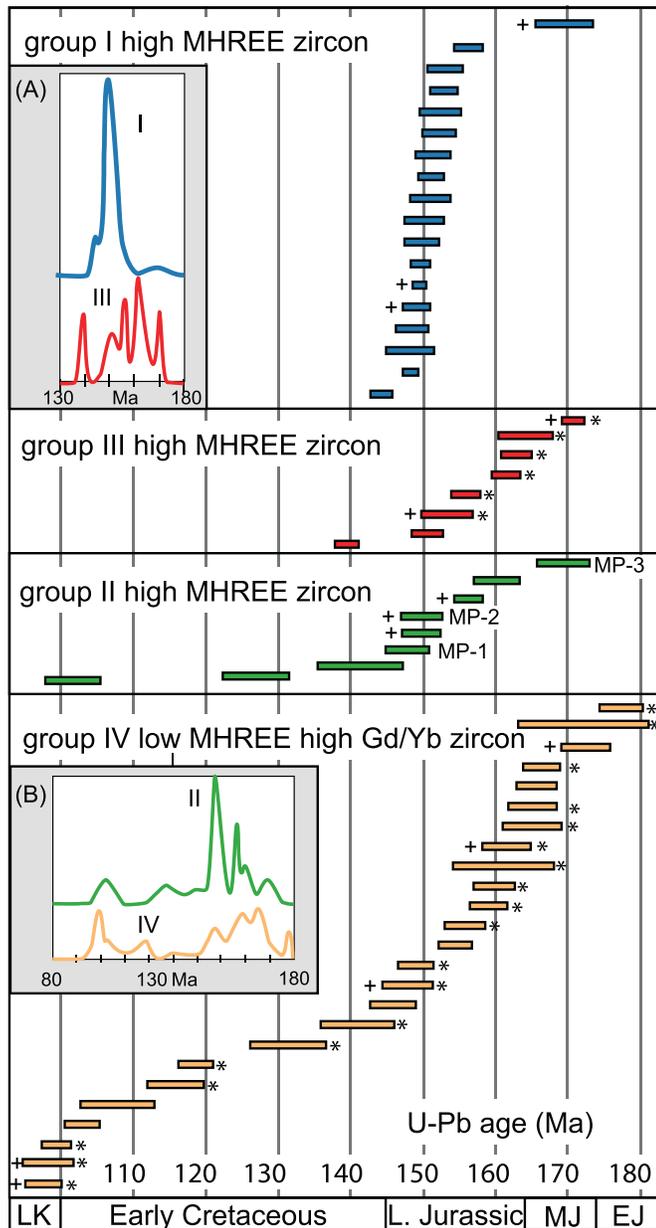
Fig. 6. U-Pb ages for high-MHREE zircon comprising groups I-III and low-REE group IV zircon. U-Pb isotopic data for forearc basin grains from Surpless et al. (2019); data for Goldstein Peak samples in ST-A. Bar lengths represent 2σ error; mean ages and probability density plots (insets) calculated using Isoplot (Ludwig, 2008). Ages of group I zircon cluster around ca. 150 Ma, with group III zircon being ca. 5–10 m.y. older. In contrast, the ages of group II and IV zircon span a nearly continuous range from Middle Jurassic through Late Cretaceous. Asterisks (right of bars) indicate zircon for which calculated magmas have concave-up MHREE patterns; plus symbols (left of bars) indicate zircon for which calculated magmas lack europium anomalies (see Fig. 12). Zircon MP-1, −2, −3 (labeled) are hypothesized as crystallizing from partial melts of Mojave province crust.

I zircons display a positive correlation between Eu/Eu* and low scandium (Sc) concentrations, implicating coupled fractionation of plagioclase and clinopyroxene (Fig. 7b).

In Fig. 8 we explore whether Nb may serve as a crude differentiation index for magmas that have not reached saturation in Nb-bearing phases (Li, Xiong & Liu, 2017; Tang et al., 2019). For example, the group I trend of decreasing Eu/Eu* due to plagioclase fractionation correlates with a Nb enrichment to ca. 55 ppm, well above the cluster of "typical" arc

zircon (Fig. 8a). A change in the fractionating assemblage may have occurred at 55 ppm Nb: above this level Eu/Eu* and Ce are relatively constant within group I, whereas Yb drops ca. 600 ppm (Fig. 8bc) and Gd drops ca. 55 ppm (not shown). The ca. 10-fold drop in Yb relative to Gd, which approximates the ratio of Yb-to-Gd garnet partition coefficients (Pertermann, Hirschmann, Hametner, Gunther & Schmidt, 2004), may mark the onset of significant igneous garnet fractionation in magmas that had differentiated to ca. 55 ppm Nb.

Not all group I zircon record increasing europium anomalies with increasing Nb contents (Fig. 8a). Plagioclase-absent clinopyroxene-garnet fractionation has been proposed to produce garnet-poor clinopyroxenite xenoliths sampled by Miocene volcanic eruptions through the west-central Sierra Nevada (Lee et al., 2006). Fractionation of HREE-depleted clinopyroxenes (Chin et al., 2012), possibly accompanied by olivine and later by garnet, could account for increases in Nb and MHREE in those group I zircon that have Eu/Eu* anomalies similar to "typical" arc zircon.

High-pressure (1.0 GPa) fractional crystallization experiments involving high-Mg basalts at reducing conditions with low initial water contents (<3%) predict fractionation of clinopyroxene and plagioclase followed by garnet. Specifically, following a period of olivine ± pyroxene fractionation, plagioclase crystallizes along with clino- and orthopyroxene in the 1140–1110 °C runs; small amounts of garnet and ilmenite first crystallize in the 1080 °C run (Ulmer et al., 2018). Even small amounts of ilmenite fractionation could explain the low Ti concentrations (av. 3.2 ppm; ST-A) of most group I zircon (Fig. 8d); alternatively, low Ti concentrations may reflect low zircon saturation temperatures (Ferry & Watson, 2007), as will be discussed further below. Late-stage ilmenite fractionation would also contribute to the low Sc concentrations characteristic of group I zircon (Fig. 7; for Sc, $Kd_{ilm-magma} = 2.6 \pm 0.4$; Klemme, Gunther, Hametner, Prowatke & Zack, 2006) but would not necessarily lower magmatic Nb contents due to neutral partition coefficients for ilmenite in basalts (1.2 ± 0.7; Klemme et al., 2006).

Our preferred scenario for group I zircon is consistent with high-pressure fractionation of high-Mg basalts in a reducing environment (Ulmer et al., 2018): (1) production of REE-enriched basalts by down-temperature fractional crystallization of olivine (± orthopyroxene) at pressures above ca. 1.0 GPa; (2) additional REE-enrichment by coupled clinopyroxene ± plagioclase fractionation, simultaneously depleting the magma in Sc and Eu^{+2} relative to Eu^{+3} while increasing magmatic Nb contents to ca. 55 ppm; (3) onset of crystallization of igneous garnet causing abrupt drops in magmatic Gd and Yb (Fig. 8c) concentrations along with a continued decrease in Sc (Fig. 7b) and a continued increase in magmatic Nb up to ca. 100 ppm; (4) possible ilmenite crystallization, which would deplete differentiating magmas in Ti; (5) Late Jurassic arc extension, liberating variably fractionated magmas produced at all stages along this fractionation pathway from the deep arc crust and possibly triggering zircon saturation at lower temperatures. This scenario is consistent with the compositions of Sierran cumulate xenoliths and MELTS modeling, both of which predict the existence of Fe and Ti-rich cumulates in the Sierran deep arc crust and connect such cumulate formation to generation of the calc-alkaline and tholeiitic arc trends (Chin, Shimizu, Bybee & Erdman, 2018; Ducea & Saleeby, 1998a). If our preferred scenario is correct, group I zircon compositions reveal how extreme fractional crystallization may generate geochemical signatures considered characteristic of unrelated tectono-magmatic settings (Grimes et al., 2015). Specifically, fractional crystallization shifted these continental arc zircons into the field of ocean island zircon on select tectonic discrimination diagrams (e.g., Fig. 2).

We singled out these experiments (i.e., fractional crystallization of high-Mg basalt under reducing conditions containing 2.0–2.6 wt.% H_2O; Ulmer et al., 2018) because the liquid line of descent matches our interpretation that plagioclase crystallization occurred early (Muntener, Keleman & Grove, 2001) relative to hornblende. Interestingly, Ulmer et al. (2018) suggest that these 1 GPa reduced, H_2O-poor (aka "damp") experiments might best apply to tholeiitic basalts
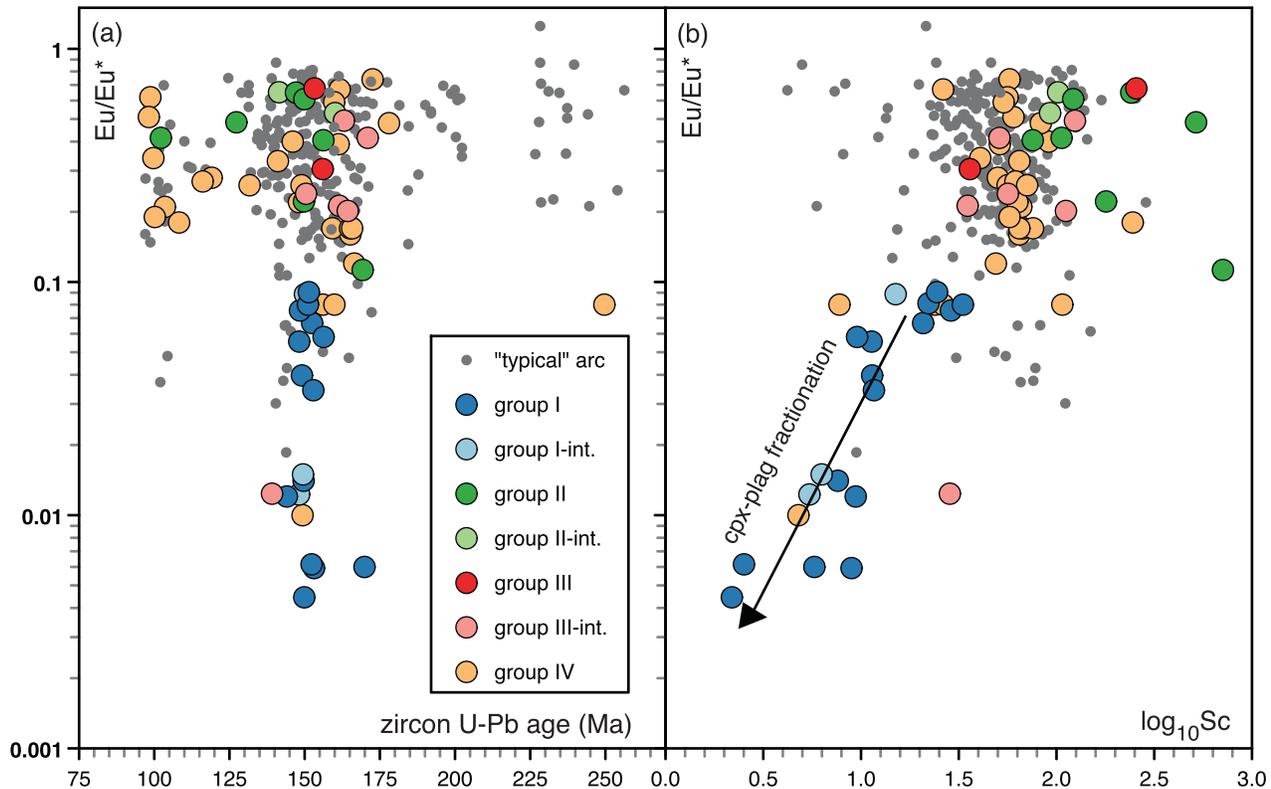
Fig. 7. Variations of the europium anomaly (Eu/Eu*) relative to zircon age and to scandium concentration (Sc). Symbols as in Fig. 4. (a) Dominantly negative log(Eu/Eu*) values indicate that Late Jurassic high-MHREE zircon crystallized from magmas that had previously crystallized plagioclase feldspar. (b) Low-Sc, group I zircon define a positive trend (arrow) indicating coupled fractionation of plagioclase feldspar and a Sc-rich phase, such as clinopyroxene. High-Sc, group II and III grains are have log(Eu/Eu*) values similar to "typical" arc zircon (gray circles). (For interpretation of the references to color in this figure legend, the reader is referred to the web version of this article.)

generated by upwelling beneath extensional arcs (e.g., Lui et al., 2020; Sisson & Bronto, 1998), a potentially appropriate scenario for the latest Jurassic Sierra Nevada arc. Despite these relatively reducing and "damp" (e.g., ca. 2% H_2O) conditions, crystallization subsequent to plagioclase+garnet+ilmenite fractionation produced a final equilibrium assemblage containing abundant hornblende (26%), one of the most general mineralogic characteristics of arc rocks. Equilibrium crystallization under oxidizing conditions results in earlier and greater total hornblende mode (52%), one of two scenarios proposed below for generating the relatively REE-poor group IV zircon.

5.2. Assimilation of Proterozoic continental and Mesozoic arc crust (group II zircon)

Group II zircons have high Sc concentrations coupled with elevated Yb that generate arc-like Sc/Yb ratios (Fig. 4a) and are further distinguished by variably high Ce concentrations and Th/U ratios (Fig. 9). Although elevated Nb concentration in group II zircons is similar to group I (Fig. 8), trace element variations within group II cannot be readily attributed to simple fractional crystallization: significant plagioclase fractionation is precluded by the "typical" arc europium anomalies of group II zircon while significant pyroxene, garnet and amphibole fractionation is precluded by the elevated Sc contents of group II zircon (Fig. 7b). Elevated Sc and REE contents might be attributed to olivine fractionation, but increased Th/U ratios cannot (Figs. 8e, 9c).

Assimilation of high Th/U and trace-element-rich crustal components, possibly occurring simultaneously with olivine fractionation, might account for the particularly high trace element contents of group II zircon. For example, significant incorporation of Proterozoic Mojave crustal province rocks has been invoked for unusual zircon compositions in eastern California magmas, including (1) high Th/U ratios (i.e.,

> 1) and Ce contents of plutonic zircon from the Mojave arc (Wooden & Miller, 1990; Wooden, Barth, & Jacobsen, 2018); (2) high coupled Th/U-Gd/Yb ratios of Mesozoic detrital zircon from the Sierra Nevada retro-arc region (Barth et al., 2013); and (3) Th/U values as high as 2.1 in Middle Jurassic volcanic zircon from the eastern Sierra Nevada arc (Barth et al., 2018). Ce enrichments in these high Th/U volcanic zircon suggest a particular kinship with group II detrital zircon. Holland et al. (2018) portray the deep footprint of the Mojave crustal province beneath the southern Sierra Nevada arc westward to the 0.706 strontium isotope isopleth, making assimilated Mojave province crust a geologically plausible component in magmatic differentiation within the southeastern Sierra Nevada arc.

We hypothesize that the high-Th/U, variably trace-element-rich compositional outliers (MP-1, -2, -3; Fig. 8) are zircon that crystallized from magmas containing a significant component of Mojave province continental crust. We use the average Th/U (0.8; $n = 53$) of high Gd/Yb (>0.07) retroarc detrital zircon (Barth et al., 2013) as an indicator of crustal input (Fig. 9). Th/U ratios of group II forearc/intra-arc detrital zircon range from 0.6 to 1.2, with half ($n = 4$) exceeding 0.8 (Fig. 9c). This high Th/U zircon subgroup includes those with both "typical" arc Nb (ca. 1–10 ppm) and Nb-rich (>40 ppm) concentrations (Fig. 8e), potentially implicating a wide range of sedimentary and volcanic rocks comprising the Mojave crustal province (Barth, Wooden, Coleman & Vogel, 2009; Strickland et al., 2013; Wooden & Miller, 1990). Production of partial melts having variably elevated Nb and Sc contents (approximated by MP-1, MP-3; Figs. 8, 9) seemingly requires melting of Nb-Sc-rich oxide minerals and/or Sc-bearing ferromagnesium silicates. In contrast, low-Nb, high Th/U crustal assimilants (approximated by MP-2; Fig. 8e) might have been high-degree partial melts of fertile Mojave province metasedimentary rocks. MP-2 plots within the cluster of "typical" arc zircon for all trace element parameters except Th/U (ca. 1.2); assimila-
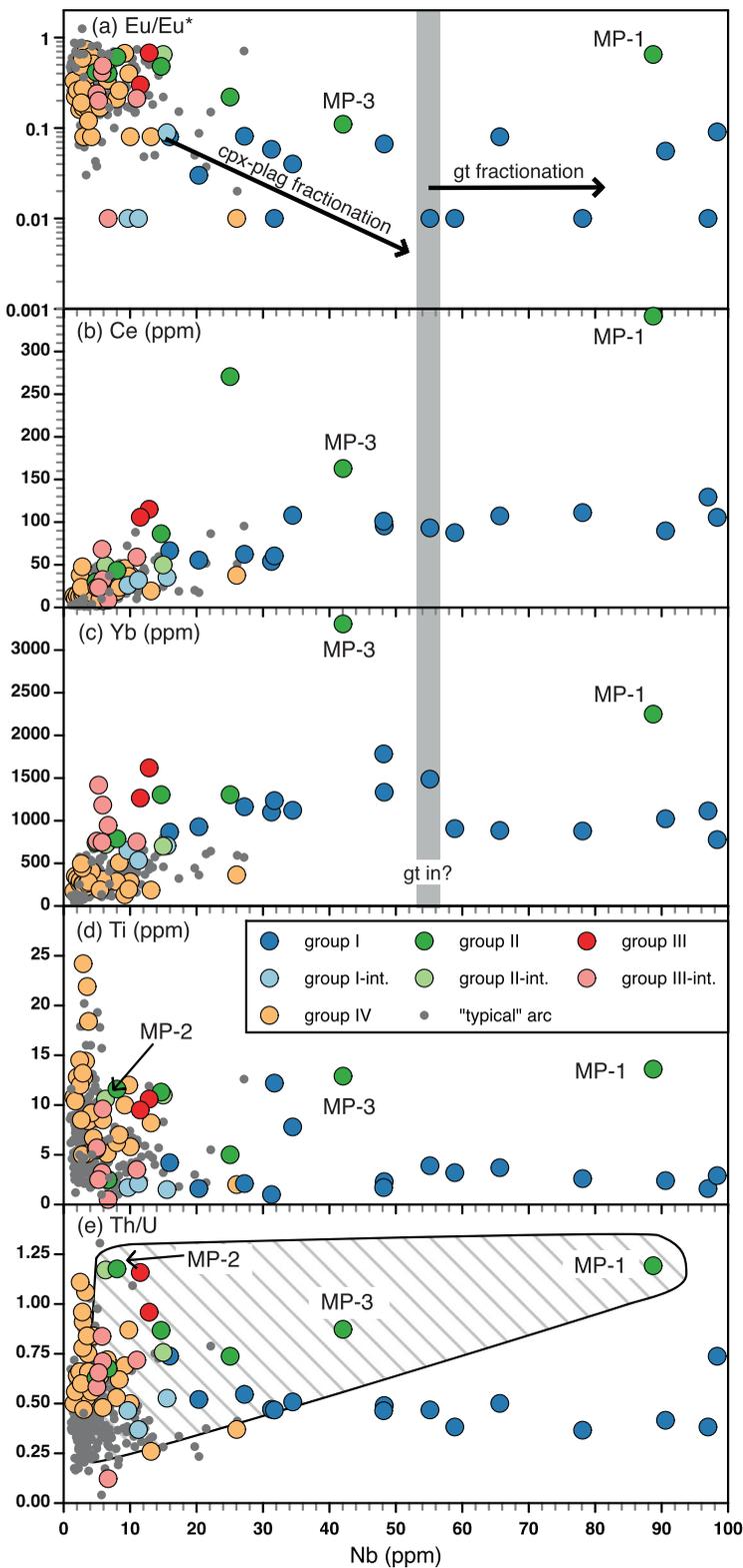
Fig. 8. Multi-parameter evaluation of Nb as a differentiation index for Late Jurassic zircon from groups I and II. (a) Group I zircon define two paths to ca. 100 ppm Nb: decreasing Eu/Eu* to ca. 55 ppm Nb (marked by gray band), followed by increasing Nb at constant Eu/Eu*; and increasing Nb at constant, arc-like Eu/Eu* and Sc. Labeled arrows indicate Nb increases potentially attributable to crystal fractionation; the "cpx-plag fractionation" arrow is comparable to that plotted on Fig. 7b, for zircon having Nb<55 ppm. No correlation exists between Eu/Eu* and elevated Nb in group II zircon. (b) Ce concentrations of group I zircon increase to 55 ppm Nb above which concentrations are unchanged; (c) group I zircon display increasing Yb to 55 ppm Nb followed by an abrupt 600 ppm drop. Elevated Yb concentrations distinguishes group III zircon from the "typical" arc cluster; (d) Ti concentrations of group I zircon fall at the low end of the "typical" arc cluster, while group II zircon labeled MP-1, −2, −3 have relatively high Ti contents; (f) group II zircon display a positive correlation between Nb and Th/U. Diagonally striped triangle depicts hypothesized mixing between low-Th/U arc magmas and magmas from which high-Th/U zircon MP-1, −2, and −3 crystallized. (For interpretation of the references to color in this figure legend, the reader is referred to the web version of this article.)

tion of such a component could produce isotopically enriched arc magmas without dramatically changing their trace element compositions. The major element compositions of these proposed Proterozoic crustal assimilants are necessarily unconstrained, but would depend largely on their mineralogy, eutectic compositions, and on the degree of partial melting.

Although any of these crustal contaminants could well be sourced directly from the lithologically diverse Mojave crustal province on which the southern arc was likely constructed, a related source is a partial melt of Mesozoic clinopyroxene+garnet+rutile arc cumulates (aka 'arclogites'; Ducea, Chapman, Bowman, & Balica, 2021). Foundering of dense arclogites into the mantle and return of some fraction to the arc crust
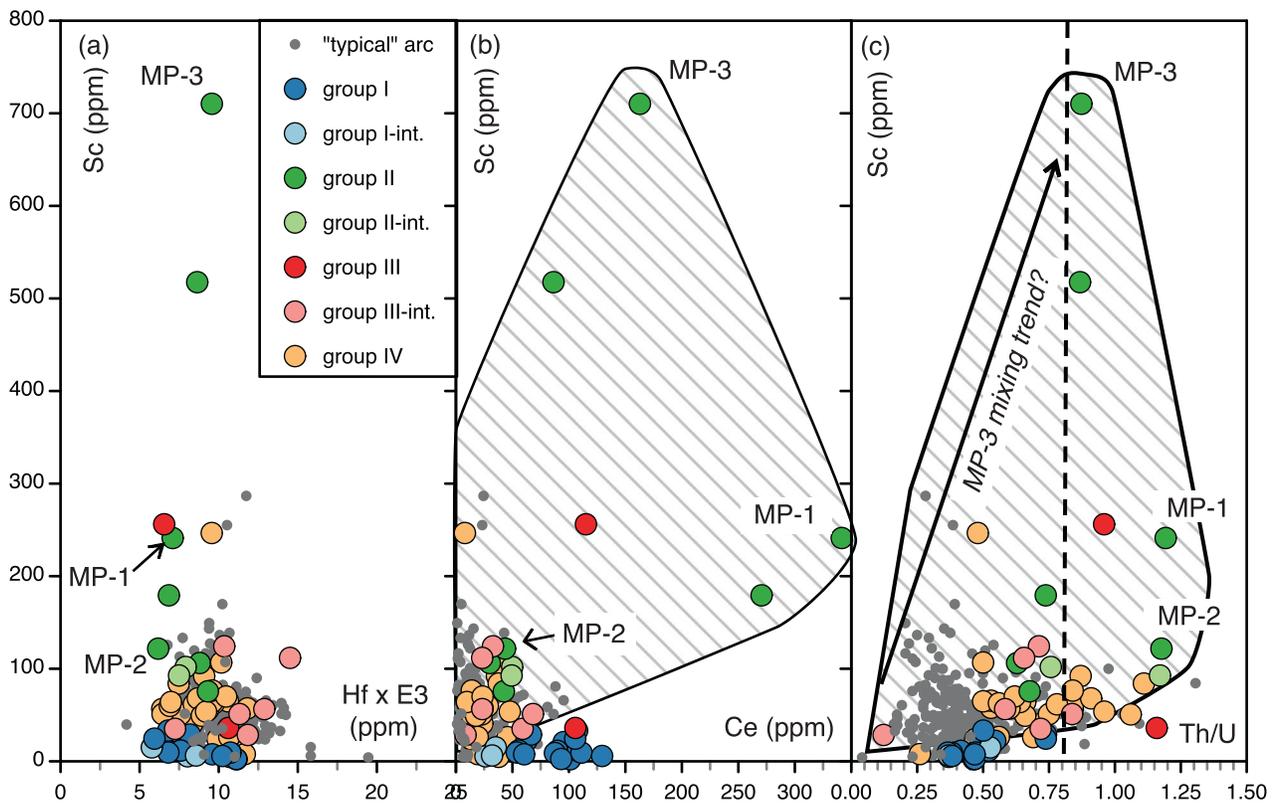
Fig. 9. Covariations between Sc with Hf, Ce and Th/U: (a) group II zircon form a linear trend that roots into the low-Hf end of the arc cluster; (b) Ce contents of group II zircon form a bimodal distribution, from arc-like to highly enriched; (c) high Th/U ratios, typically > 0.8, potentially indicating zircon crystallization from mafic to intermediate magmas containing a significant component of partial melts derived from the Mojave crustal province. Zircon labeled MP-1 (147.1 ± 1.9 Ma) and MP-2 (149.9 ± 2.8 Ma) crystallized from magmas rich in the hypothetical high- and low-Nb, high Th/U crustal contaminants (Fig. 8d). High Th/U zircon MP-3 (169.3 ± 3.4 Ma; ST-A) has the highest Sc concentration. Diagonally striped polygons depict hypothesized mixing between low-Th/U arc magmas and high-Th/U crustal melts (MP-1,−2,−3). (For interpretation of the references to color in this figure legend, the reader is referred to the web version of this article.)

via partial melting is hypothesized to play a key role in the genesis of continental crust (Saleeby, Ducea & Clemens-Knott, 2003). Such partial melts are predicted to be Ti- and Nb-rich, due to fusion of rutile and Fe-Ti oxides (Tang et al., 2019); high Sc and Yb contents (e.g., MP-3) are consistent with partial melting of clinopyroxene-garnet-rutile assemblages. For Sierran arclogites, high-Th/U ratios might reflect an original assimilated component of Mojave crustal province preserved in the cumulate protoliths; later cumulate delamination and partial melting could return the crustal signature to younger arc magmas (Ducea & Saleeby, 1998b). The moderately elevated Th/U (0.89) of MP-3 might also record production of a garnet-rich residue during high-pressure partial melting of arclogite, due to the slightly greater affinity shown by garnet for U relative to Th (Kd$_{garnet-basalt}$ = 0.0017 for Th; Kd$_{garnet-basalt}$ = 0.0015 for U; LaTourrette, Kennedy & Wasserburg, 1993).
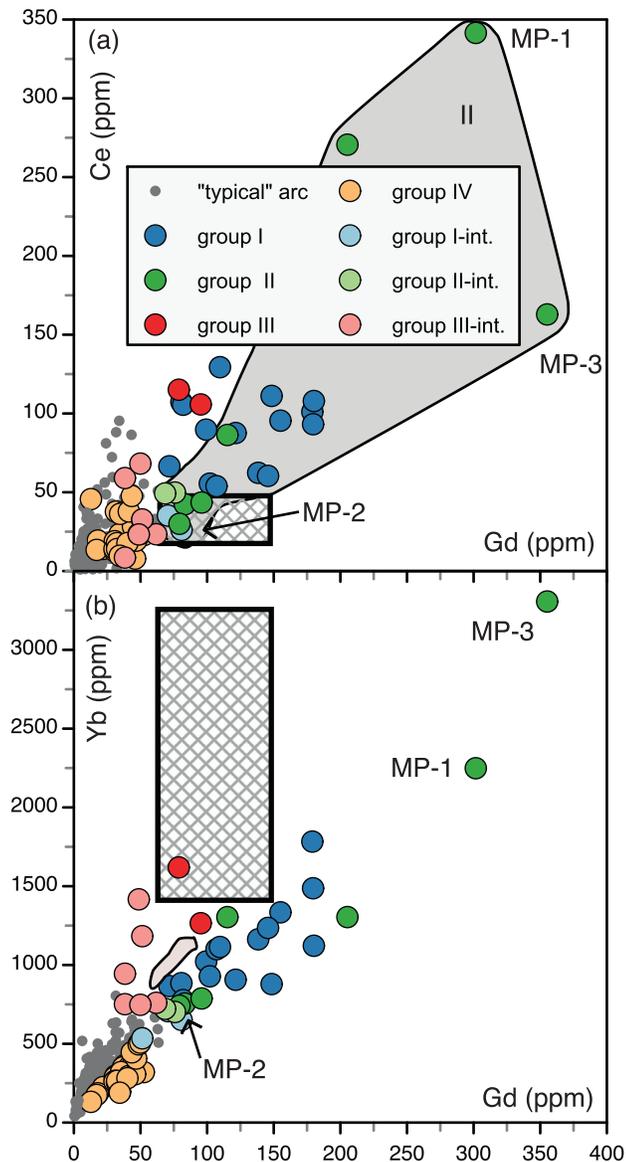
Variable incorporation of some Sc-rich partial melt into arc magmas is shown in Figs. 9abc by a smattering of otherwise "typical" arc zircon that have elevated Sc concentrations, pulling them away from the "typical" arc cluster towards MP-3. Group II forms a linear Hf-Sc trend that roots into the low-Hf (<10,000 ppm) end of the "typical" arc cluster, suggesting that group II zircon are mixtures between relatively mafic, low-Hf arc magmas and the proposed high Th/U assimilants (approximated by MP-1, −2, and −3; Fig. 9a), a concept illustrated by speculative Th/U-Nb-Sc-Ce mixing triangles (Figs. 8e, 9bc). High Ti concentrations of zircon MP-1, −2, and −3 (Fig. 8d) implicate relatively high temperatures of zircon saturation, consistent with partial melting of either deep continental crust or foundered arclogites. Heat balance considerations make it likely that crustal assimilation was coupled with fractional crystallization: limited plagioclase fractionation may be recorded by the small negative Eu anomalies of group II zir-

con (Fig. 8b); olivine fractionation would increase magmatic REE contents without leaving another trace element record. Repeated recharge and mixing in a mixing-assimilation-storage-homogenization (MASH; Hildreth & Moorbath, 1988) zone mutes most individual signals of fractionating mineral phases. Our preferred interpretation is that group II zircon crystallized from magmas produced in a MASH zone near the base of the arc crust by interaction between a variety of partial melts of Mojave crustal province rocks and mantle-derived magmas. The latter includes both basaltic partial melts of the mantle wedge and intermediate partial melts of foundered Mesozoic arclogites (Ducea, Chapman, Bowman, & Balica, 2021).

5.3. Depressurization reactions (group III zircon)

The magnitude of REE enrichment relative to the dense cluster of "typical" arc zircon increases from group III to group I to group II (Fig. 10a). Whereas groups I and II display co-linear Ce-Gd-Yb enrichments, group III zircon are disproportionately enriched in Yb relative to Gd (Fig. 10b). Fractionation of Gd from Yb suggests involvement of hornblende, an abundant, REE-rich silicate in Sierra Nevada arc plutons in which Gd is more compatible than Yb (Sisson, 1994).

In their trace element study of hornblende crystals from Late Jurassic plutons of the Klamath arc in northern California, Barnes, Berry, Barnes and Ernst (2017) proposed that green magnesiohornblende rims grew on brown tschermakitic-to-magnesiohornblende crystals that were partially resorbed during depressurization. These authors calculated magma compositions from which the green hornblende rims might have crystallized, noting that such magmas would have concave-upwards-shaped REE patterns (aka "reverse-J" patterns) that are atypically en-

ARTICLE IN PRESS

JID: RINGEO
[m5GeSdc;August 10, 2021;13:6]

D. Clemens-Knott, K.D. Surpless, A.P. Barth et al.
Results in Geochemistry xxx (xxxx) xxx

Fig. 10. Covariation of Gd (MREE) concentration with (a) Ce (LREE), and (b) Yb (HREE). Group I and II zircon are proportionally REE-enriched relative to "typical" arc zircon, with high Th/U zircon MP-1 and MP-3 having the highest REE values. Cross-hatched rectangles demark the compositional ranges of zircon (18–49 ppm Ce; 69–150 ppm Gd; 1500–3200 ppm Yb; calculations in ST-E) predicted to crystallize from magmas generated by decompression reactions between brown hornblende and upwelling host magmas (Barnes et al., 2017). Eight Jurassic, high-MHREE volcanic zircon preserved in intra-arc strata plot within the group III field (small gray oval; Attila et al., 2020). Symbols as in Fig. 4. (For interpretation of the references to color in this figure legend, the reader is referred to the web version of this article.)

riched in heavy REE (e.g., Yb). In other words, upwelling-induced resorption of high-temperature (ca. 880–780 °C) brown hornblende phenocrysts that originally crystallized at mid-crustal depths (ca. 18 km) generated transient magmas that were REE-enriched and had particularly low Gd/Yb ratios due to unusually high Yb contents. Zircon crystallizing simultaneously with the lower temperature (ca. 750 °C) green hornblende rims presumably would preserve these atypical Gd/Yb ratios along with an overall REE-enrichment generated by resorption of brown hornblende, matching the general character of group III zircon.

The dominantly Middle to Late Jurassic ages of Sierran high-MHREE zircon (Fig. 6) suggest a possible connection with magma upwelling dur-

ing arc transtension as ultimately recorded by emplacement of the Independence dike swarm. To test whether group III zircon might have crystallized from transient magmas generated by brown hornblende resorption, we apply zircon-magma distribution coefficients (Sano, Terada & Fukuoka, 2002) to the calculated magmatic REE compositions of Barnes et al. (2017) in order to predict the compositional range of zircon crystallizing along with green hornblende rims (ST-E). Notably, group III zircon trend towards the calculated range of zircon Gd-Yb contents (diagonal patterned box, Fig. 10b); the Ce contents of group II zircon, however, are higher than predicted for this process, which we attribute to Ce-rich assimilants (e.g., MP-1, MP-3).

U-Pb ages of group III zircon (Fig. 6) span ca. 10 m.y. prior to the ca. 148 Ma emplacement of the Independence dike swarm, potentially recording the earliest stages of extension-induced mobilization of magmas from the middle arc crust. Based on the atypical enrichment of Yb relative to Gb in these Middle to Late Jurassic zircon, we propose that group III zircon crystallized from geochemically transient magmas generated by partial resorption of hornblende phenocrysts during extension-induced magma upwelling. If the Sierran and Klamath arcs were similarly constructed, then group III likely documents crystallization of brown hornblende at mid-crustal depths, consistent with many predictions, models, and observations for the Sierra Nevada arc (e.g., Blatter, Sisson & Hankins, 2013; Sisson et al., 1996). A large volcanic zircon database from central Sierran pendants ($n = 1099$; Attila et al., 2020) contains only 8 Jurassic high-MHREE zircon, all of which plot within the group III field (Fig. 10b). Resorption of hornblende phenocrysts during magmatic upwelling preceding volcanic eruptions is consistent with the depressurization model.

Barnes et al. (2017) report elevated Nb contents for green hornblende rims (19–41 ppm; RBEP024; $n = 6$; ST-D) relative to all other Klamath analyses (ave. = 13 ppm; $n = 323$), implying that the transient magmas were enriched in Nb. If so, simultaneous crystallization of group III zircon with Nb-rich green hornblende rims predicts that group III zircon would also have elevated Nb, but instead Nb concentrations of group III zircon (5–13 ppm) are similar to "typical" arc zircon (Fig. 8). Crystallization of low-Nb group III zircon from presumably Nb-rich magmas may be explained by the high average amphibole-magma partition coefficient for Nb (6.6; Humphreys et al., 2019a,b; ST-D) calculated for Klamath arc green hornblende rims (Barnes et al., 2017) relative to low zircon-magma distribution coefficients for Nb (0.15–0.7; Chapman, Gehrels, Ducea, Giesler & Pullen, 2016; Grimes et al., 2015). These partition coefficients combine to predict a ca. 10 to 40-times-enrichment of Nb in green hornblende rims relative to zircon when these phases crystallize simultaneously from transient Nb-enriched magmas. Thus, the transient magma may indeed have been Nb-rich due to decompression resorption of brown hornblende, but the crystallizing green hornblende out-competed group III zircon for Nb. MHREE partition coefficients for zircon and green hornblende predict a ca. 14 times enrichment in zircon Yb relative to coeval green hornblende (Kd$_{zircon-magma}$ ca. 277 for Yb, Sano et al., 2002; calculated Kd$_{green\ hornblende-magma}$ for Yb of 20, see ST-D) consistent with the observed Yb-rich compositions of group III zircon (Fig. 10b).

5.4. Low REE, high Gd/Yb zircon (group IV zircon)

Our analysis reveals a fourth geochemically distinct population of zircon having REE contents similar to "typical" arc zircon but with Gd/Yb ratios consistent with crystallization from magmas produced at elevated pressure in the presence of either igneous or metamorphic garnet. Gd/Yb ratios of group IV zircon are similar to those of groups I and II, all of which are higher than the "typical" arc zircon preserved in Sierran forearc, intra-arc (> 0.1; Figs. 4b, 5b) and retro-arc basins (Fig. 11b). Group IV is further distinguished by containing the most Ti-rich zircon, implicating relatively high temperatures of zircon saturation (Fig. 11a). The presence of hornblende as a fractionating phase with group IV zircon (average Sc/Yb = 0.23) is supported by the conclusion that zircon
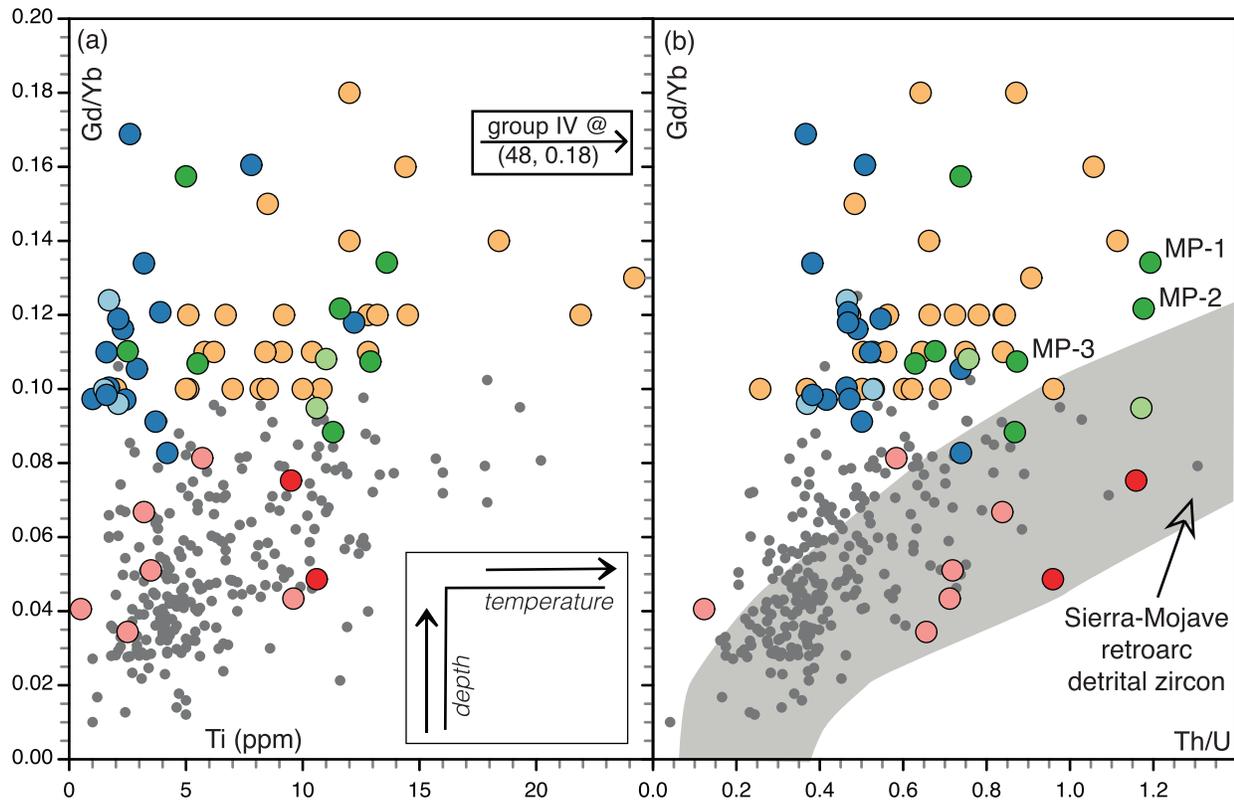
Fig. 11. Covariation of Gd/Yb with (a) Ti, and (b) Th/U: (a) Ti contents of high Gd/Yb groups I, II and IV range from low (group I) to high (group IV). Group III is indistinguishable from "typical" arc zircon. (b) The field of Sierra/Mojave retroarc zircon (light gray field, after Barth et al., 2013) is shown for comparison to forearc/intra-arc zircon groups I-IV. Groups I, II and IV have higher Gd/Yb than both "typical" forearc and retroarc zircon; group III zircon have lower Gd/Yb than most "typical" arc zircon but overlap the retroarc zircon field. Symbols as in Fig. 10. (For interpretation of the references to color in this figure legend, the reader is referred to the web version of this article.)

Sc/Yb ratios exceeding 0.1 reflect the presence of fractionating amphibole (Grimes et al., 2015) and by their low overall REE contents that are similar to "typical" arc zircon (Fig. 3). Moreover, calculated partition coefficients indicating high REE compatibility for the majority of Jurassic hornblende from the Klamath arc are consistent with our hypothesis that hornblende played a significant role in depleting arc magmas in REE prior to and during crystallization of "typical" arc zircon: average amphibole-magma $Kd_{Ce} = 3.0$, $Kd_{Gd} = 15.2$, $Kd_{Yb} = 8.0$ (see "all other amphibole analyses" in ST-D; data from Barnes et al., 2017; equations from Humphreys et al., 2019a,b).

Group IV zircon range from Early Jurassic to Early Cretaceous age (Fig. 6) and span a range of Sc-REE-Hf contents and Eu/Eu* and Th/U ratios nearly equivalent to the entire cluster of "typical" arc zircon (e.g., Figs. 7b, 8). This geochemical diversity, along with indications of relatively high-temperature (i.e., high Ti), high-pressure (i.e., high Gd/Yb) crystallization, is consistent with models for arc recycling in the deep Sierran lithosphere (Ducea & Saleeby, 1998b). Specifically, low-REE group IV zircon may have crystallized from moderately high-volume partial melts of the arc itself, including (1) ultramafic cumulates represented by garnet-clinopyroxene-rutile arclogite xenoliths that may have formed during generation of low-Mg gabbros found at high levels of the arc (Ducea, Chapman, Bowman, & Balica, 2021; Lee et al., 2006; Tang et al., 2019); (2) gabbroic cumulates, crystallization of which produced the highly fractionated magmas from which group I zircon crystallized; and (3) tonalitic to granitic arc rocks transported to partial melting depths by return flow, magmatic inflation, or underthrusting (Chin et al., 2012; DeCelles, Ducea, Kapp & Zandt, 2009).

High-pressure fractionation of hornblende in the presence of garnet prior to zircon saturation provides an alternative and/or complementary origin for group IV zircon. When conducted under oxidizing conditions, fractional crystallization experiments of high-Mg basalts and basaltic andesites demonstrate significant crystallization of hornblende prior to plagioclase, garnet and ilmenite (Ulmer et al., 2018). As argued above, hornblende fractionation may be largely responsible for the relatively low-REE contents of "typical" arc zircon, while garnet fractionation would produce a high Gd/Yb signal in any group IV zircon that subsequently crystallized.

6. Discussion

Zircon trace elements provide crude proxies for zircon crystallization depth (i.e., Gd/Yb), zircon saturation temperature (i.e., Ti) and contamination by ancient continental crust (i.e., high Th/U). Covariations between these proxies emphasize the unusual compositions of zircons from high-MHREE groups I and II, along with low-REE group IV, relative to the "typical" compositions of zircon erupted and eroded from the upper arc and preserved as detrital zircon in forearc, intra-arc and retroarc basins (dark gray circles and light gray field; Fig. 11). For example, the high Gd/Yb and Th/U ratios coupled with moderately high Ti contents of group II zircon are consistent with differentiation of parental magmas in deep crustal MASH magma chambers in which mantle-derived magmas interacted with hot partial melts of the Mojave crustal province. Group III zircon differ from those in group II by having lower Gd/Yb ratios, consistent with the possibility that the evacuation of hornblende-phyric magmas from deep crustal MASH zones produced the group III zircon having Th/$U > 0.8$.

However, the low Ti concentrations (and implied low zircon saturation temperatures) of group I zircons are not consistent with our model of crystallization in deep, hot MASH chambers. Two possible explanations exist for this discrepancy: (1) group I zircon crystallized

in the cool, upper crust, after Late Jurassic extension evacuated highly fractionated parental magmas from deep crustal magmas chambers; or (2) low-Ti group I zircon crystallized at depth from magmas that had previously fractionated ilmenite, consistent with the experiments of Ulmer et al. (2018); ca. 1080 °C at 1 GPa. Ilmenite fractionation prior to zircon crystallization can be accommodated by the Ti-in-zircon thermometer by reducing magmatic a_{TiO2} to reflect the resulting magmatic Ti-depletion (Ferry & Watson, 2007), but too many melt parameters are unconstrained for detrital zircon making a unique interpretation impossible. It is feasible that both ilmenite fractionation in the lower crust combined with some cooling in the upper crust produced the magmas from which low-Ti group I zircon crystallized.

Seen in the context of these geochemical proxies, low-REE group IV zircon apparently crystallized from magmas that interacted with Proterozoic crust and/or partial melts of early Mesozoic arclogite to an extent similar to combined groups I and II.

6.1. Calculated melt compositions

We explore these petrologic interpretations by calculating the compositions of parental magmas in equilibrium with group I-IV zircon. Empirical correlations between zircon Ti and REE contents determined for volcanic zircon-glass pairs can be leveraged to calculate compositions of melts from which zircon crystallized (Claiborne et al., 2018; ST-C). We note that this approach assumes (1) that changes in zircon trace element compositions are controlled by the temperature-dependence of zircon-magma partition coefficients; and (2) that these empirical equations do not accommodate down-temperature adjustments to a_{TiO2} and a_{SiO2} that might be appropriate for magmas that experienced ilmenite fractionation (e.g., group I). Calculated magma compositions erase the portion of the Eu anomaly intrinsic to the chondrite-normalized REE patterns of zircon (Bea et al., 1994), allowing any remaining Eu/Eu* anomaly to be attributed to plagioclase fractionation.

Calculated REE trends for group I and IV magmas that lack marked Eu anomalies are comparable to those of magmas from the Cascade arc (gray band in Fig. 12a; Bacon et al., 1997), lending credence to these empirical calculations. Smooth, LREE-enriched patterns calculated for three group I and four group II zircons may have been produced by high-temperature olivine ± pyroxene fractionation from mafic magmas that had not yet become saturated in plagioclase + garnet. Alternatively, smooth LREE-enriched patterns may be produced by partial melting of almost any silicate rock, in which the greater incompatibilities of the LREE in most rock-forming silicate minerals result in LREE-enriched magmas. Possible examples of partial melts include magmas calculated from two of the three high Th/U zircon (MP-1, MP-2) of group II that may have originated as partial melts of Mojave province metamorphic rocks or early Mesozoic arclogites, as well as five group IV magmas, tentatively attributed to recycling of arc plutonic rocks. Shown for comparison is the calculated magma for the most REE-poor zircon in the entire forearc + intra-arc database (GP-03_5.1; ST-A); this calculated magma has a flat REE pattern consistent with zircon crystallization from a partial melt of depleted mantle. Calculated trace element contents of zircon-saturated arc magmas plot intermediate between partial melts of depleted-mantle and ancient continental crust (e.g., MP-1, MP-2). These calculations suggest that some group III magmas included a larger mantle component, relative to some group II magmas that included a larger crustal component.

Pronounced negative Eu anomalies are displayed by the remaining group I magmas (*n* = 15), consistent with significant fractional crystallization of a plagioclase-bearing assemblage (Fig. 12b). Combined with an HREE depletion implicating garnet fractionation, the calculated REE trends are consistent with our interpretation that the majority of group I zircon owe their extreme REE contents to pronounced crystal fractionation of olivine+clinopyroxene+plagioclase+garnet ±ilmenite deep in the arc crust. The calculated parental magma for Sc-rich zircon MP-3 ('MP-3 magma') and for the 2 group II magmas also have negative

Eu/Eu*, possibly recording plagioclase fractionation within the proposed MASH environment.

The majority of calculated group III magmas (Fig. 12c) display the distinctive concave-up MHREE pattern attributed to arc magmas mobilized upwards by arc rifting that have partially resorbed high-pressure hornblende (Barnes et al., 2017). Most group III magmas display moderate Eu anomalies, implicating coupled plagioclase-hornblende crystallization prior to zircon saturation. In addition, the majority of magmas calculated for low-REE group IV zircon also display concave-up MHREE patterns (Fig. 12ad). Group IV zircon were identified based on the high Gd/Yb values relative to the "typical" cluster of arc zircon (Fig. 4b), and indeed some of these calculated group IV liquids retain high Gd/Yb consistent with garnet crystallization. Combined with strong negative Eu anomalies displayed by most group IV magmas, we interpret this subset of calculated parental magmas as fractionating hornblende at high pressures in addition to plagioclase and garnet. Hornblende fractionation would deplete magmas in REE, especially the MHREE, potentially masking any trace element record of olivine and/or clinopyroxene fractionation at higher temperatures as well as producing low-REE magmas from which the low-REE group IV zircon subsequently crystallized. 1 GPa fractional crystallization experiments of high-Mg basalts and basaltic andesites under oxidizing conditions demonstrate significant crystallization of hornblende prior to plagioclase, garnet and ilmenite (Ulmer et al., 2018). Subsequent depressurization and hornblende resorption could produce the concave-up Yb enrichment seen in the majority of calculated group IV magmas, whereas others retained the low-Yb signal of garnet fractionation. Calculated liquids thus indicate two possible origins for this group IV zircon: (IV-i) those lacking significant Eu anomalies may have crystallized from partial melts of a variety of recycled arc rocks including arclogites (Fig. 12a); and (IV-ii) those having significant Eu anomalies may have crystallized from differentiates formed by high-pressure fractional crystallization of hornblende-plagioclase-garnet under oxidizing conditions (Fig. 12d).

The calculated REE contents of parental magmas for high-MHREE group I zircon and low-REE group IV zircon are surprisingly similar, regardless of whether calculated magmas have Eu anomalies (Fig. 12bd) or not (Fig. 12a). This similarity seemingly negates our hypothesis for REE-depletion by hornblende fractionation prior to crystallization of group IV zircon. One possibility is that the elevated MHREE contents of group I zircon might be explained by crystallization in the cool, upper crust after Late Jurassic evacuation of their hot, deep crustal chambers. In this scenario, the low Ti contents of group I zircon (Fig. 8d) truly reflect low crystallization temperatures, and the effective large magma-zircon partition coefficients produced REE-rich group I zircon from otherwise typical low-REE arc magmas. However, at low crystallization temperatures the increased magma-zircon partition coefficient for Sc should also result in Sc-rich zircon, in marked contrast to the characteristic low Sc content of group I zircon. An alternative scenario is that low Ti contents of group I zircon primarily reflect crystallization from REE-rich, highly differentiated magmas that had substantially lower Ti due to ilmenite fractionation, as implicated by high-pressure experiments (Ulmer et al., 2018). We illustrate the potential impact of Ti depletion by artificially enriching group I zircon in Ti (see figure caption), which predictably results in more REE-rich calculated magmas for group I zircon (gray field, Fig. 12d). Although we cannot preclude the possibility that all of the trace element variations we document result from increasing partition coefficients due to dramatically decreased temperature of zircon saturation, it seems improbable that fractional crystallization would generate the wide range of Sc (behaving as a compatible element in the fractionating assemblage) and Nb (seemingly behaving as an incompatible element) concentrations recorded by group I zircon (Figs. 6, 7) without also generating atypically REE-rich magmas. We infer that the crystallization histories of magmas from which group I zircon crystallized were likely in between these endmember scenarios, leaving the degree of magmatic REE-enrichment by pronounced high-pressure fractional crystallization unconstrained.

D. Clemens-Knott, K.D. Surpless, A.P. Barth et al.
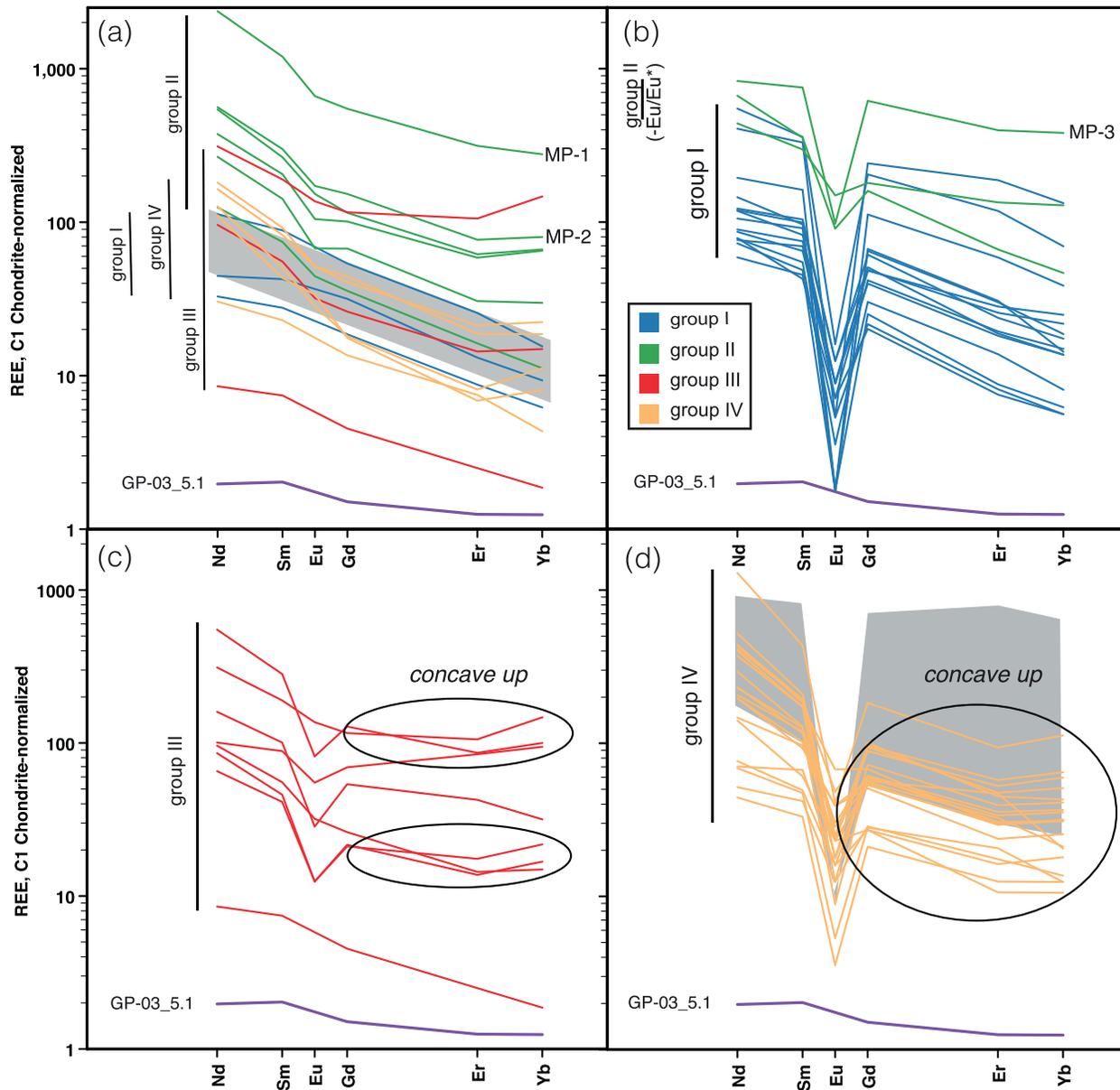
Fig. 12. Chondrite-normalized rare earth element plots for liquids calculated using empirical equations of Claiborne et al. (2018); ST-B). Subhorizontal REE pattern for liquid calculated from zircon GP-03_5.1 (purple) is shown as an approximation of mantle-derived arc magma. (a) Calculated liquids lacking significant europium anomalies, including possible lower crustal partial melts MP-1 and MP-2. Group I (blue); group II (green); group III (red); group IV (orange). Gray band highlights REE contents of average Cascade arc magmas (Bacon et al., 1997). (b) Remaining liquids calculated for group I (blue) and II (green) zircon, including possible lower crustal melt MP-3. (c) All calculated group III liquids, most of which display concave-up MHREE patterns consistent with hornblende resorption due to depressurization reaction (Barnes et al., 2017). (d) Liquids calculated for group IV zircon not plotted in 11a, many of which display concave-up MHREE patterns. The gray field depicts the REE range of group I magmas calculated using Ti concentrations increased by a factor of 3.5, the difference between the average Ti contents of group I and IV zircon. (For interpretation of the references to color in this figure legend, the reader is referred to the web version of this article.)

If these interpretations of calculated magma compositions are indeed applicable to zircon genesis, the main difference between groups I and IV zircon is due either to zircon saturation temperature (i.e., group IV zircon crystallized in the hot, deep crust, whereas group I zircon crystallized after parental magmas migrated to the cool upper crust), or to whether hornblende crystallized in the deep crust prior to zircon saturation (group IV-ii) or not (group I). Factors influencing high-pressure hornblende fractionation include whether crystallization from high-Mg basalt occurred under oxidizing (group IV-ii) or reducing (group I) conditions in the deep arc crust (Ulmer et al., 2018), and whether crystallization occurred during fractionation of high-Mg basalt (group I) or high-Mg basaltic andesite (group IV-ii). Likely variations in parental magma composition, oxygen fugacity and crystallization temperature within long-lived arcs thus preclude unique interpretations of group I and IV zircon genesis.

6.2. Conceptual model

We summarize our model for the origins for groups I-IV zircon in a schematic cross-section (Fig. 13). Central to this model is the hypothesis that Late Jurassic SW-NE crustal transtension mobilized deep arc differentiates and facilitated evolution of geochemically atypical arc magmas by decompression resorption of hornblende. The majority of calculated liquids displaying concave-up MHREE patterns (Fig. 12cd for
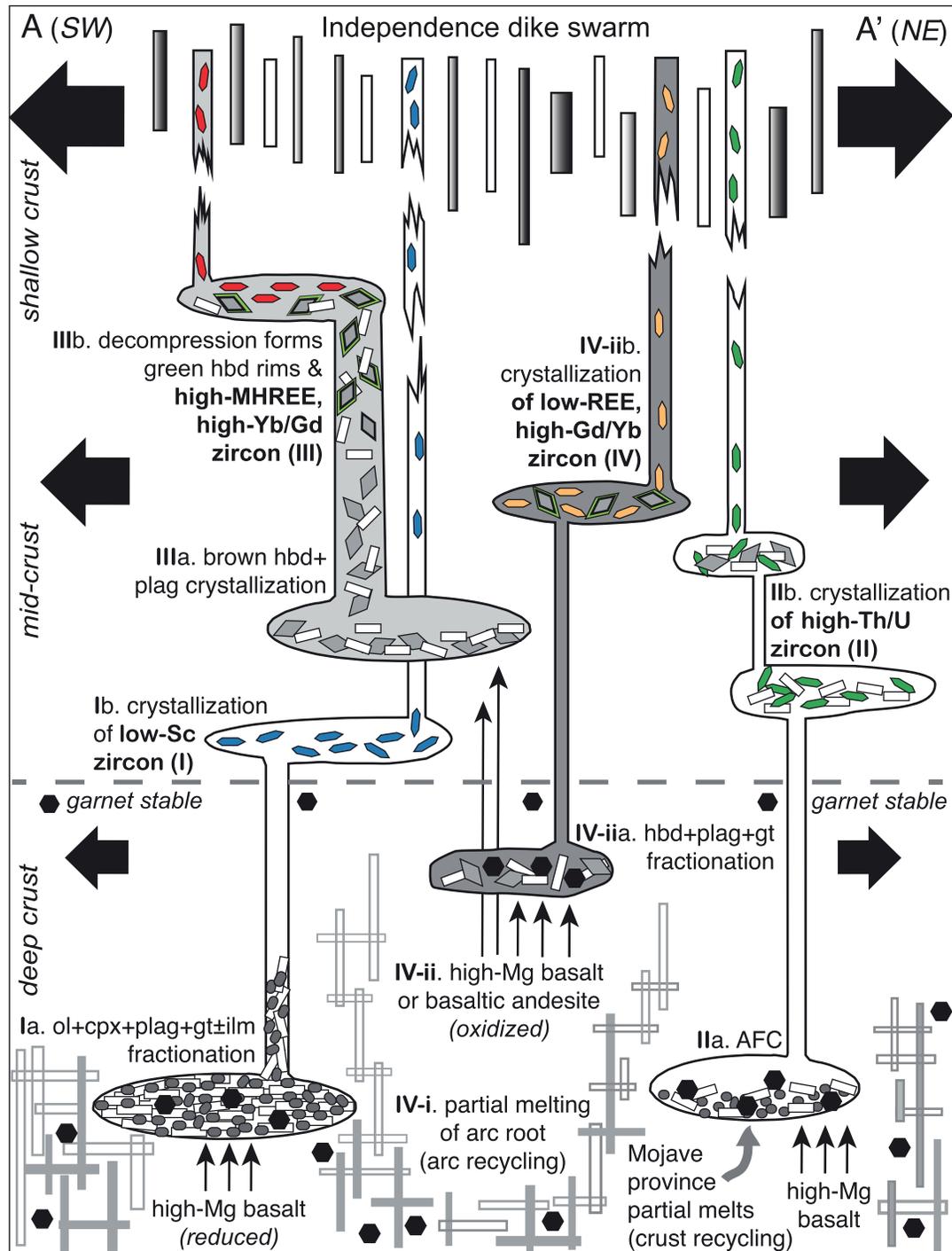
Fig. 13. Conceptual model of five magmatic differentiation pathways coexisting in the middle-to-deep arc crust that we hypothesize were mobilized by Middle to Late Jurassic SW-NE crustal extension (thick black arrows). Cross-section line A-A' (Fig. 1) is oriented perpendicular to the trend of the Late Jurassic Independence dike swarm. Ia: fractional crystallization of olivine+clinopyroxene+plagioclase from reduced, high-Mg basalt, followed by garnet and potentially ilmenite fractionation in deep crustal chambers. Ib: evacuation of Sc-depleted, REE-enriched residual magma having a negative europium anomaly, and subsequent crystallization of low-Sc, high-MHREE group I zircon. IIa: assimilation-fractional crystallization (AFC) between mantle-derived arc basalts and partial melts of garnetiferous Mojave crustal province rocks. IIb: crystallization of high Th/U, high-MHREE group II zircon from MASH differentiates. IIIa: crystallization of brown hornblende in mid-crustal chambers. IIIb: depressurization reaction between brown hornblende and host magma during rapid, extension-driven upwelling generates green hornblende rims and calculated parental magmas having concave-up MHREE patterns from which the high Yb/Gd, high-MHREE group II zircon crystallized. IV-i: crystallization of high-Gd/Yb, low-REE group IV zircon from partial melts of garnetiferous arc plutonic rocks, including arclogites, which had previously been transferred downwards into the arc's growing lithospheric root; magmatic differentiation pathways are unconstrained for this group so are not depicted. IV-iia: fractional crystallization of high-Mg basalt to basaltic andesite under oxidizing conditions, fractionating hornblende-plagioclase-garnet. IV-iib: depressurization reaction between brown hornblende and host magma during rapid, extension-driven upwelling generates calculated parental magmas having concave-up REE patterns from which the high Gd/Yb, low-REE group IV zircon crystallized. Symbols and abbreviations: plagioclase (plag; white rectangles); clinopyroxene (cpx; gray ovals); garnet (gt; black hexagons); zircon (prisms, colored by group as in Fig. 12); brown hornblende (hbd; light gray diamonds); green amphibole rims (light green diamonds); ilmenite (ilm). Olivine fractionation is unconstrained by zircon trace element compositions so is not depicted. Tartan-pattern (dark to light gray rectangles near lower edge) within garnet stability field (area below dashed gray line) represents a dike-and-sill complex of mantle-derived basalts and partial melts of the lithospheric root; variably evolved, zircon-bearing Independence dikes (vertical white-to-black rectangles) emplaced into shallow arc crust at ca. 150 Ma. (For interpretation of the references to color in this figure legend, the reader is referred to the web version of this article.)

zircon groups III, IV) are Middle to Late Jurassic age (asterisks, Fig. 6) supporting a possible down-from-the-top opening of the arc crust, with relatively shallower, hornblende-phyric magmas (groups III, IV-ii) rising earlier than those sequestered at depth (groups I, II, IV-i). This temporal interpretation is consistent with 1 GPa experiments indicating a ca. 200 °C difference between high-pressure crystallization conditions for rock-forming silicate assemblages with which group IV-ii (900–720 °C) and group I (1080 °C) zircon crystallized. Enhanced buoyancy of hornblende-saturated magmas may have contributed to this age trend, with groups III and IV rising faster than groups I and II.

Group I: Fractional crystallization of olivine, clinopyroxene, plagioclase, and lesser garnet and ilmenite (Ia; Fig. 13) formed peridotitic to gabbroic cumulates and extremely fractionated magmas from which these low-Sc, low-Eu/Eu*, high-MHREE zircon crystallized (Ib; Fig. 13). Elevated REE contents argue against substantial magmatic crystallization of garnet, which would efficiently deplete a host magma in MHREE. Though the early crystallization of plagioclase may reflect fractional crystallization under relatively reduced conditions of high-Mg tholeiitic magmas underplated due to arc extension (Ulmer et al., 2018), the ca. 150 Ma age of group I zircon indicates that these fractionated magmas escaped the deep arc crust only with the aid of crustal extension. Recall that group I zircon are the only type of high-MHREE zircon that have not yet been identified in other arcs (Fig. 5). Regardless of the parental magma composition, we speculate that in the absence of a significant extensional event, such high-MHREE magmas might crystallize in situ largely as intercumulus hornblende, possibly never reaching zircon saturation or physically trapping any group-I-like zircon in mafic cumulates within the arc root.

Group II: Assimilation of high-Th/U partial melts of Mojave province mafic igneous and metasedimentary rocks by low-Hf, mantle-derived basaltic magmas and/or intermediate partial melts of foundered arclogite (IIa; Fig. 13) produced MASH differentiates from which high-REE group II zircon crystallized (IIb; Fig. 13). Repeated recharge of various trace-element-rich magmas may mute most signals of fractionating mineral phases, other than the distinctive signals of plagioclase (Eu/Eu*) and garnet (high Gd/Yb) fractionation. The wide range of group II ages suggest that zircon saturation of these MASH differentiates was independent of crustal extension, although ascent through the thick arc lithosphere may have been facilitated by both Middle (ca. 165 Ma) and Late Jurassic extension.

Group III: Mid-crustal crystallization of brown hornblende (IIIa; Fig. 13), which was subsequently destabilized and resorbed during decompression reactions, produced low Gd/Yb, high-MHREE melts from which both green hornblende rims and group III zircon crystallized (IIIb; Fig. 13). The Middle to Late Jurassic ages of group III zircon suggest that upwelling of hornblende-porphyritic magmas preceded and coincided with emplacement of the Independence dike swarm.

Group IV: We portray two possible origins: (1) partial melting of deep arc lithosphere in the presence of garnet produced zircon-saturated intermediate magmas that bore a wide range of trace element signatures generated during earlier cycles of arc magmagenesis (subgroup IV-i; Fig. 13). High-temperature partial melts of foundered clinopyroxene-garnet-rutile arclogites are possible members of this subgroup; and (2) fractionation of hornblende, plagioclase and garnet from mafic magmas under oxidizing conditions prior to zircon saturation (subgroup IV-ii, stage a; Fig. 13), followed by crystallization of low-REE, high Gd/Yb zircon at mid-crustal levels (IV-ii, stage b; Fig. 13). Experimental results indicate significantly lower crystallization temperatures for the hornblende-bearing mineral assemblages accompanying subgroup IV-ii zircon than those accompanying group I zircon, implicating shallower depths within the garnet stability field for differentiation of subgroup IV-ii magmas. The wide age range of subgroup IV-i zircon (+ symbols in Fig. 6) suggest that buoyant zircon-bearing partial melts of deep arc lithosphere might have been incorporated into mid- to upper-crustal magma mush systems through much of the Mesozoic.

6.3. Age and tectono-magmatic considerations

Although we focused this study on largely Late Jurassic zircons with anomalous trace element compositions, we infer that the differentiation processes we identify, excepting decompression reactions in hornblende-phyric magmas, operated during most of the Mesozoic lifespan of the arc. We attribute the apparent dearth of similarly anomalous zircon of Triassic or Cretaceous age to sampling and preservation constraints. Most anomalous zircons formed during the Late Jurassic Independence dike swarm transtensional event, suggesting that (Middle to) Late Jurassic arc extension evacuated deep arc chambers prior to significant hornblende crystallization, permitting fractionated and AFC-differentiated magmas and their zircon cargoes the opportunity to traverse the thick arc crust. These magmas either erupted to form volcanic tephra, a record of which is preserved in intra-arc basins (Attila et al., 2020) and in far-field basins east of the arc (Christiansen et al., 2015; Kowallis, Christiansen, Deino, Zhang & Everett, 2001), or were emplaced into the shallow arc crust, which facilitated their relatively rapid erosion. Middle to Late Jurassic ages of group III zircon may record the mobilization and ascent of hornblende-porphyritic, intermediate magmas from the middle crust ca. 5 to 10 m.y. prior to the upper crustal emplacement of the Independence dike swarm.

The relatively wide range of ages for groups II and IV zircon (Fig. 6) indicate that the garnet-present generation of MHREE-rich magmas in deep crustal MASH zones and relatively REE-poor magmas either by partial melting of arc lithosphere or by hornblende-plagioclase-garnet fractionation was not limited to Late Jurassic time. Group IV zircons may have been integrated into buoyant, intermediate magma batches that successfully intruded the arc upper crust independent of Late Jurassic extension. However, the ca. 150 Ma age peak present in both groups (inset, Fig. 6) may indicate that Late Jurassic extension also facilitated the ascent of these zircon-bearing magmas.

Middle to Late Jurassic detrital zircons have a high likelihood of preservation in the latest Jurassic to Early Cretaceous arc-proximal extensional basins that served as traps for these anomalous zircon (Clemens-Knott et al., 2013b; Orme & Surpless, 2019). We conclude that atypical magmas were evacuated by arc rifting and their anomalous trace element characteristics preserved in detrital zircon within arc-proximal grabens, together emphasizing the importance of extension within the Middle to Late Jurassic Sierra Nevada arc in first releasing REE-rich magmas then capturing detrital records of deep arc crustal processes.

6.4. Geochemical basis for trace element tectonic discrimination

Group I high-MHREE zircon from our forearc/intra-arc detrital zircon database display the low Sc/Yb character generally associated with both plume and MORB zircon (Fig. 2). We conclude that the low Sc/Yb character of group I zircon relative to the continental arc field is due largely to fractional crystallization. This anomalous low Sc/Yb (and high [Yb]) signature would be largely erased once fractionating magmas became saturated in hornblende, because both Yb and Sc are compatible in hornblende. Our model accounts for all geochemically anomalous high-MHREE zircon by invoking reasonable differentiation pathways within the arc crust (Fig. 13) and eliminates the need to invoke geochemically anomalous mantle sources. Plagioclase crystallization is typically suppressed in plume magmagenesis due to high pressures, such that low-Sc/Yb continental arc zircon might be distinguished from true plume zircon by their large negative europium anomalies (Fig. 7b).

7. Conclusions

Middle to Late Jurassic extension in the southern Sierra Nevada arc released variably fractionated magmas from the middle to deep arc lithosphere, the compositions of which are recorded in unusual high-MHREE zircons (group I-III zircon) and low-REE but atypically high

Gd/Yb zircons (group IV). Geochemical analysis of these atypical detrital zircon grains, coupled with calculated REE compositions of their parental melts, provides a rare view into deep arc differentiation pathways. Ca. 150 Ma zircon crystallization (group I) from magmas produced by extensive olivine+clinopyroxene+plagioclase+garnet±ilmenite fractionation suggests that the host magmas escaped the deep crust cumulate chambers at the climax of Late Jurassic extension and reached zircon saturation prior to hornblende saturation. Middle to Late Jurassic extension similarly evacuated partial melts of the high Th/U Mojave crustal province along with MASH differentiates (group II). Mid-crustal hornblende-phyric magmas experienced depressurization during this period; resorption of Nb-Sc-REE-rich hornblende produced transient magmas that imparted their concave-up MHREE pattern on the high Yb/Gd zircon that subsequently crystallized (group III). Lastly, differentiation under more oxidizing conditions than experienced by group I was driven by fractionation of hornblende+plagioclase+garnet. This differentiation pathway, possibly coupled with partial melting of pre-existing arc products including foundered arclogite, may have produced buoyant low-REE magmas that successfully reached the upper arc crust throughout the time interval recorded by these Early Jurassic to Early Cretaceous zircon.

These geochemically anomalous detrital zircon record Jura-Cretaceous crustal growth (e.g., differentiation of mafic to intermediate magmas) and crustal recycling (e.g., partial melting of Proterozoic Mojave crust and/or arclogites). Such differentiation processes have previously been deduced from the geochemistry of compositionally evolved continental arc rocks, evaluated with experimental data, and integrated in petrogenetic models for continental margin arc magmatism. Our results from detrital zircon preserved in forearc and intra-arc strata provide further evidence for the roles of these processes in producing geochemically differentiated magmas deep in the arc root thereby demonstrating the success of this analytical strategy. Additionally, our results provide new insights into Sierra Nevada magmatism tied to arc rifting: the predominantly Middle to Late Jurassic ages of the high-MHREE, high Gd/Yb zircon implicate magma mobilization from deep in the arc root; a subset of high Yb/Gd zircon may record modification of magma compositions by decompression resorption of high-pressure hornblende; and the reduced conditions of high-pressure crystallization implicated by early plagioclase fractionation may identify a period of tholeiitic magmatism accompanying Jurassic arc rifting (Ulmer et al., 2018).

Because arc extension may promote evacuation of geochemically anomalous magmas resident in the deep arc lithosphere, recognition of geochemically anomalous, plume-like zircon (e.g., group I) and other high-MHREE zircon (e.g., groups II and III) may help identify previously unrecognized extensional events in lesser studied arcs. In the case of the Sierra Nevada, we interpret zircons having elevated MHREE, Nb and Sc contents as having crystallized from differentiated magmas mobilized from the deep arc lithosphere by Late Jurassic extension. Our results demonstrate that analysis of geochemically anomalous detrital zircon preserved in arc-proximal basins provides a revealing window into deep-arc magmatic processes.

Declaration of Competing Interest

The authors declare that they have no known competing financial interests or personal relationships that could have appeared to influence the work reported in this paper.

Supplementary materials

Supplementary material associated with this article can be found, in the online version, at doi:10.1016/j.ringeo.2021.100010.

References

Attila, S., Cottle, J. M., & Paterson, S. R. (2020). Erupted zircon record of continental crust formation during mantle driven arc flare-ups. *Geology, 48*, 446–451.

Bacon, C. R., Bruggman, P. E., Christiansen, R. L., Clynne, M. A., Donnelly-Nolan, J. M., & Hildreth, W. (1997). Primitive magmas at five Cascade volcanic fields: Melts from hot, heterogeneous sub-arc mantle. *The Canadian Mineralogist, 35*, 397–423.

Barker, S. J., Wilson, C. J. N., Smith, E. G. C., Charlier, B. L. A., Wooden, J. L., Hiess, J., et al. (2014). Post-supereruption magmatic reconstruction of Taupo Volcano (New Zealand), as reflected in zircon ages and trace elements. *Journal of Petrology, 55*, 1533.

Barnes, C. G., Berry, R., Barnes, M. A., & Ernst, W. G. (2017). Trace element zoning in hornblende: Tracking and modeling the crystallization of a calc-alkaline arc pluton. *American Mineralogist, 102*(12), 2390–2405.

Barth, A. P., Feilen, A. D. G., Yager, S. L., Douglas, S. R., Wooden, J. L., Riggs, N. R., et al. (2012). Petrogenetic connections between ash-flow tuffs and a granodioritic to granitic intrusive suite in the Sierra Nevada arc, California. *Geosphere, 8*, 250–264.

Barth, A. P., Walker, J. D., Wooden, J. L., Riggs, N. R., & Schweickert, R. A. (2011). Birth of the Sierra Nevada magmatic arc: Early Mesozoic plutonism and volcanism in the east-central Sierra Nevada of California. *Geosphere, 7*(4), 877–897.

Barth, A. P., Wooden, J. L., Coleman, D. S., & Vogel, M. B. (2009). Assembling and disassembling California: A zircon and monazite geochronologic framework for Proterozoic crustal evolution in southern California. *The Journal of Geology, 117*, 221–239.

Barth, A. P., Wooden, J. L., Jacobson, C. E., & Probst, K. (2004). U-Pb geochronology and geochemistry of the McCoy Mountains Formation, southeastern California: A Cretaceous retroarc foreland basin. *Geological Society of America Bulletin, 116*(1/2), 142–153.

Barth, A. P., Wooden, J. L., Miller, D. M., Howard, K. A., Fox, L. K., Schermer, E. R., et al. (2017b). Regional and temporal variability of a Cordilleran magma pulse: Age and chemical evolution of the Jurassic arc, eastern Mojave Desert, California. *Geological Society of America Bulletin, 129*, 429–448.

Barth, A. P., Wooden, J. L., Riggs, N. R., Walker, J. D., Tani, K., Penniston-Dorland, S. C., …, & H. iramatsu, R. (2018). Marine volcaniclastic record of early arc evolution in the eastern Ritter Range pendant, central Sierra Nevada, California. *Geochemistry Geophysics Geosystems, 19*, 2543–2559.

Barth, A., & Wooden, J. (2010). Coupled elemental and isotopic analyses of polygenetic zircons from granitic rocks by ion microprobe, with implications for melt evolution and the sources of granitic magmas. *Chemical Geology, 277*(1–2), 149–159.

Barth, A., Wooden, J., Jacobson, C., & Economos, R. (2013). Detrital zircon as a proxy for tracking the magmatic arc system: The California arc example. *Geology, 41*, 223–226.

Barth, A. P., Tani, K., Meffre, S., Wooden, J. L., Coble, M. A., Arculus, R. J., …, & S. hukle, J. T. (2017a). Generation of silicic melts in the early Izu-Bonin arc recorded by detrital zircons in proximal arc volcaniclastic rocks from the Philippine Sea. *Geochemistry, Geophysics Geosystems, 18*, 3576–3591. 10.1002/2017GC006.

Bateman, P. C. (1992). Plutonism in the central part of the Sierra Nevada batholith, California. *U.S. Geological Survey Professional Paper, 1483*.

Bea, F., Pereira, M. D., & Stroh, A. (1994). Mineral/leucosome trace-element partitioning in a peraluminous migmatite (a laser ablation-ICP-MS study). *Chemical Geology, 114*, 291–312.

Black, L. P., Kamo, S. L., Allen, C. M., Davis, D. W., Aleinikoff, J. N., Valley, J. W., et al. (2004). Improved $^{206}Pb/^{238}U$ microprobe geochronology by the monitoring of a trace-element-related matrix effect: SHRIMP, ID-TIMS, ELA-ICP-MS, and oxygen isotope documentation for a series of zircon standards. *Chemical Geology, 205*, 115–140.

Blatter, D. L., Sisson, T. W., & Hankins, W. B. (2013). Crystallization of oxidized, moderately hydrous arc basalt at mid- to lower-crustal pressures: Implications for andesite genesis. *Contributions to Mineralogy and Petrology, 166*, 861–886.

Busby, C. J., Schermer, E. R., & Mattinson, J. M. (2002). Extensional arc setting and ages of Middle Jurassic eolianites, Cowhole Mountains (eastern Mojave Desert block, California). In A. F. Glazner, J. D. Walker, & J. M. Bartley (Eds.), *Geologic Evolution Of The Mojave Desert And Southwestern Basin And Range* (pp. 79–91). Geological Society of America Memoir. Vol. 195.

Busby-Spera, C. J. (1988). Speculative tectonic model of the early Mesozoic arc of the southwest Cordilleran United States. *Geology, 16*, 1121–1125.

Busby-Spera, C. J., Mattinson, J. M., Riggs, N. R., & Schermer, E. R. (1990). The Triassic-Jurassic magmatic arc in the Mojave-Sonoran deserts and the Sierran-Klamath region: Similarities and differences in paleogeographic evolution. In D. S. Harwood, & M. M. Miller (Eds.), *Paleozoic and Early Mesozoic Paleogeographic Relations; Sierra Nevada, Klamath Mountains*. And Related Terranes: Boulder, Colorado Geological Society of America Special Paper 255.

Cao, W., Paterson, S. R., Memeti, V., Mundil, R., Anderson, L., & Schmidt, K. (2015). Tracking paleodeformation field in a continental arc: A study of incremental and finite strain in Mesozoic plutons and host rocks, respectively in central Sierra Nevada, California. *Lithosphere, 7*(3), 296–320. 10.1130/L389.1.

Carl, B. S., & Glazner, A. F. (2002). *Extent And Significance Of The Independence Dike Swarm, Eastern California, Geologic Evolution Of The Mojave Desert And Southwestern Basin And Range, Volume Geological Society Of America Memoir 195* (pp. 117–130). Geological Society of America.

Carley, T. L., Miller, C. F., Wooden, J. L., Padilla, A. J., Schmitt, A. K., Economos, R. C., et al. (2014). Iceland is not a magmatic analog for the Hadean: Evidence from the zircon record. *Earth and Planetary Science Letters, 405*, 85–97.

Chamberlain, K. J., Wilson, C. J. N., Wooden, J. L., Cherlier, B. L. A., & Ireland, T. R. (2014). New perspectives on the Bishop Tuff from zircon textures, ages and trace elements. *Journal of Petrology, 55*, 95–426.

Chapman, J. B., Gehrels, G. E., Ducea, M. N., Giesler, N., & Pullen, A. (2016). A new method for estimating parent rock trace element concentrations from zircon. *Chemical Geology, 439*, 59–70.

Chen, J. H., & Moore, J. G. (1979). Late Jurassic Independence Dike Swarm in Eastern California. *Geology, 7*, 129–133.

Chin, E. J., Lee, C. T. A., Luffi, P., & Tice, M. (2012). Deep lithospheric thickening and refertilization beneath continental arcs: Case study of the P, T and compositional evolution of peridotite xenoliths from the Sierra Nevada. *California: Journal of Petrology, 53*(3), 477–511.

Chin, E. J., Lee, C. T. A., & Tollstrup, D. (2013). On the origin of hot metasedimentary quartzites in the lower crust of continental arcs. *Earth and Planetary Science Letters, 361*, 120–133.

Chin, E. J., Shimizu, K., Bybee, G. M., & Erdman, M. E. (2018). On the development of the calc-alkaline and tholeiitic magma series. *A deep crustal cumulate perspective: Earth and Planetary Science Letters, 482*, 277–287.

Christiansen, E. H., Kowallis, B. J., Dorais, M. J., Hart, G. L., Mills, C. N., Pickard, M., et al. (2015). The record of volcanism in the Brushy Basin Member of the Morrison FOrmation: Implications for the Late Jurassic of western North America. In T. H. Anderson, A. N. Didenko, C. L. Johnson, A. I. Khanchuk, & J. H. MacDonald (Eds.), *Late Jurassic Margin Of Laurasia—A Record Of Faulting Accommodating Plate Rotation* (pp. 399–439). Geological Society of America. Special Paper 513. 10.1130/2015.2513(11).

Claiborne, L. L. (2011). *Understanding Upper Crustal Silicic Magmatic Systems Using The Temporal, Compositional And Thermal Record In Zircon* (p. 375). Nashville, Vanderbilt University.

Claiborne, L. L., Miller, C. F., Guillherme, A. R., Gualda, Carley, T., L., Covey, A. K., et al. (2018). Zircon as magma monitor: Robust, temperature-dependent partition coefficients from glass and zircon surface and rim measurements from natural systems. In D. E. Moser, F. Corfu, J. R. Darling, S. M. Reddy, & K. Tait (Eds.), *Microstructural Geochronology: Planetary Records Down To Atom Scale, Geophysical Monograph v. 232*. American Geophysical Union. John Wiley & Sons, Inc.

Clemens-Knott, D., & Saleeby, J. B. (2013a). Mesozoic metasedimentary framework and gabbroids of the Early Cretaceous Sierra Nevada batholith, California. In K. Putirka (Ed.), *Geological Society Of America Field Guide, v. 32* (pp. 79–98). Boulder, CO, United States: Geological Society of America.

Clemens-Knott, D., van der Kolk, D. A., Sturmer, D. M., & Saleeby, J. B. (2013b). The Goldstein peak formation, central California: Record of a nonmarine intra-arc basin within the Early Cretaceous Sierra Nevada arc. *Geosphere, 9*(4), 718–735.

Coble, M. A., Vazquez, J. A., Barth, A. P., Wooden, J., Burns, D., Kylander-Clark, A., et al. (2018). Trace element characterization of MAD-559 zircon reference material for ion microprobe analysis. *Geostandards and Geoanalytical Research, 42*, 481–497.

Coleman, D. S., & Glazner, A. F. (1997). The Sierra Crest magmatic event: Rapid formation of juvenile crust during the late Cretaceous in California. *International Geology Review, 39*(9), 768–787.

Colgan, J., & Stanley, R. (2016). The Point Sal–Point Piedras Blancas correlation and the problem of slip on the San Gregorio–Hosgri fault, central California Coast Ranges. *Geosphere, 12*(3), 971–984.

DeCelles, P. G., Ducea, M. N., Kapp, P., & Zandt, G. (2009). Cyclicity in Cordilleran orogenic systems. *Nature Geoscience*, (2), 251–257.

DeGraaff-Surpless, K., Graham, S. A., Wooden, J. L., & McWilliams, M. O. (2002). Detrital zircon provenance analysis of the Great Valley Group, California: Evolution of an arc-forearc system. *Geological Society of America Bulletin, 114*(12), 1564–1580.

Dilles, J. H., Kent, A. J., Wooden, J. L., Tosdal, R. M., Koleszar, A., Lee, R. G., et al. (2015). Zircon compositional evidence for sulfur-degassing from ore-forming arc magmas. *Economic Geology, 110*, 241–251.

Ducea, M. N., Chapman, A. D., Bowman, E., & Balica, C. (2021). Arclogites and their role in continental evolution: Part 2: Relationship to batholiths and volcanoes, density and foundering, remelting and long-term storage in the mantle. *Earth-Science Reviews, 214*. 10.1016/j.earscirev.2020.103476.

Ducea, M. N., & Saleeby, J. (1998a). The age and origin of a thick mafic-ultramafic keel from beneath the Sierra Nevada batholith. *Contributions to Mineralogy and Petrology, 133*, 169–185.

Ducea, M. N., & Saleeby, J. (1998b). Crustal recycling beneath continental arcs: Silica-rich glass inclusions in ultramafic xenoliths from the Sierra Nevada, California. *Earth and Planetary Science Letters, 156*, 101–116.

Dunne, G. C., & Walker, J. D. (2004). Structure and evolution of the East Sierran thrust system, east central California. *Tectonics, 23*(4), TC4012.

Ferrari, L., Petrone, C. M., & Francalanci, L. (2001). Generation of oceanic-island basalt–type volcanism in the western Trans-Mexican volcanic belt by slab rollback, asthenosphere infiltration, and variable flux melting. *Geology, 29*(6), 507–510 n..

Ferry, J. M., & Watson, E. B. (2007). New thermodynamic models and revised calibrations for the Ti-in-zircon and Zr-in-rutile thermometers. *Contributions to Mineralogy and Petrology, 154*, 429–437.

Gaetani, G. A., & Grove, T. L. (1998). The influence of water on melting of mantle peridotite. *Contributions to Mineralogy and Petrology, 131*, 323–346.

Glazner, A. F., Bartley, J. M., & Carl, B. S. (1999). Oblique opening and noncoaxial emplacement of the Jurassic Independence dike swarm. *California: Journal of Structural Geology, 21*, 1275–1283.

Glazner, A. F., Carl, B. S., Coleman, D. S., Miller, J. S., & Bartley, J. M. (2008). Chemical variability and the composite nature of dikes from the Jurassic Independence dike swarm, eastern California, Ophiolites, Arcs, and Batholiths. *A Tribute to Cliff Hopson*, 445–480.

Grimes, C. B., John, B. E., Kelemen, P. B., Mazdab, F. K., Wooden, J. L., Cheadle, M. J., et al. (2007). Trace element chemistry of zircons from oceanic crust: A method for distinguishing detrital zircon provenance. *Geology, 35*, 643–646.

Grimes, C. B., Wooden, J. L., Cheadle, M. J., & John, B. E. (2015). Fingerprinting" tectono–magmatic provenance using trace elements in igneous zircon. *Contributions to Mineralogy and Petrology, 170*, 46.

Hildreth, W., & Moorbath, S. (1988). Crustal contributions to arc magmatism in the Andes of Central Chile. *Contributions to Mineralogy and Petrology, 98*, 455–489.

Hirt, W. H. (2007). Petrology of the Mount Whitney Intrusive Suite, eastern Sierra Nevada, California: Immplications for the emplacement and differentiation of composite felsic intrusions. *GSA Bulletin, 119*, 1185–1200.

Holland, M. E., Karlstrom, K. E., Gehrels, G., Shufeldt, O. P., Begg, G., Griffin, W., et al. (2018). The Paleoproterozoic Vishnu basin in southwestern Laurentia: Implications for supercontinent reconstructions, crustal growth, and the origin of the Mojave crustal province. *Precambrian Research, 308*, 1–17.

Humphreys, M. C. S., Cooper, G. F., Zhang, J., Loewen, M., Kent, A. J. R., Macpherson, C. G., et al. (2019a). Unraveling the complexity of magma plumbing at Mount St. Helens: A new trace element partitioning scheme for amphibole. *Contributions to Mineralogy and Petrology, 174*, 1–17.

Humphreys, M. C. S., Cooper, G. F., Zhang, J., Loewen, M., Kent, A. J. R., Macpherson, C. G., et al. (2019b). Unraveling the complexity of magma plumbing at Mount St. Helens: A new trace element partitioning scheme for amphibole. *Contributions to Mineralogy and Petrology, 174*(1), 1–15.

Ingersoll, R. V. (1983). Petrofacies and provenance of late Mesozoic forearc basin, northern and central California. *AAPG Bulletin, 67*(7), 1125–1142.

James, E. W. (1989). Southern extension of the Independence dike swarm of eastern California. *Geology, 17*, 587–590.

James, O. (1971). Origin and emplacement of the ultramafic rocks of the Emigrant Gap area, California. *Journal of Petrology, 12*, 523–560.

Kistler, R. W., & Peterman, Z. E. (1973). Variations in Sr, Rb, K, Na, and initial Sr87/Sr86 in Mesozoic granitic rocks and intruded wall rocks in central California. *GSA Bulletin, 84*, 3489–3512.

Klemme, S., Gunther, D., Hametner, K., Prowatke, S., & Zack, T. (2006). The partitioning of trace elements between ilmenite, ulvospinel, armalcolite and silicate melts with implications for the early differentiation of the moon. *Chemical Geology, 234*, 251–263.

Kowallis, B. J., Christiansen, E. H., Deino, A. L., Zhang, C., & Everett, B. H. (2001). The record of Middle Jurassic volcanism in the Carmel and Temple Cap Formations of southwestern Utah. *GSA Bulletin, 113*, 373–387.

LaTourrette, T. Z., Kennedy, A. K., & Wasserburg, G. J. (1993). Thorium-uranium fractionation by garnet: Evidence for a deep source and rapid rise of oceanic basalts. *Science (New York, N.Y.), 261*, 739–742.

Lee, C. T. A., Cheng, X., & Horodyskyj, U. (2006). The development and refinement of continental arcs by primary basaltic magmatism, garnet pyroxenite accumulation, basaltic recharge and delamination: Insights from the Sierra Nevada, California. *Contributions to Mineralogy and Petrology, 151*, 222–242.

Li, L., Xiong, X. L., & Liu, X. C. (2017). Nb/Ta fractionation by amphibole in hydrous basaltic systems: Implications for arc magma evolution and continental crust formation. *Journal of Petrology, 58*, 3–28.

Linn, A. M., DePaolo, D. J., & Ingersoll, R. V. (1991). Nd-Sr isotopic provenance analysis of upper cretaceous great valley fore-arc sandstones. *Geology, 19*(8), 803–806.

Ludwig, K. (2008). Isoplot 3.6: Berkeley Geochronology Center Special Publication 4, 77 p.

Lui, Z., Di-Cheng, Z., Jagoutz, O., Rezeau, H., Wang, Q., & Eyuboglu, Y. (2020). Magmatic evolution following damp tholeiitic and wet calc-alkaline liquid lines of descent: An Eastern Pontides (NE Turkey) example. *Journal of Petrology*. 10.1093/petrology/egaa088.

Martin, M. W., & Clemens-Knott, D. (2015). Detrital-zircon record of the early Mesozoic southwestern Sierra Nevada arc preserved in Lower Cretaceous intra-arc and forearc deposits of central California. In T. H. Anderson, A. N. Didenko, C. L. Johnson, A. I. Khanchuk, & J. H MacDonald (Eds.), *Late Jurassic Margin Of Laurasia—A Record Of Faulting Accommodating Plate Rotation* (pp. 269–284). Denver, CO: Geological Society of America. Geological Society of America Special Paper 513, Vol. 513.

Mazdab, F. K., & Wooden, J. L. (2006). Trace element analysis in zircon by ion microprobe (SHRIMP-RG): *Technique and Applications: Geochimica et Cosmochimica Acta, 70*(18), A405 -A405.

Memeti, V., Paterson, S., Matzel, J., Mundil, R., & Okaya, D. (2010). Magmatic lobes as "snapshots" of magma chamber growth and evolution in large, composite batholiths: An example from the Tuolumne intrusion, Sierra Nevada, California. *Geological Society of America Bulletin, 122*, 1912–1931.

Mullen, E. K., Weis, D., March, N. B., & Martindale, M. (2017). Primitive arc magma diversity: New geochemical insight in the Cascade Arc. *Chemical Geology, 448*, 43–70.

Muntener, O., Kelemen, P. B., & Grove, T. L. (2001). The role of H_2O during crystallization of primitive arc magmas under uppermost mantle conditions and genesis of igneous pyroxenites: An experimental study. *Contributions to Mineralogy and Petrology, 141*, 643–658.

Nandedkar, R. H., Hurlimann, N., Ulmer, P., & Muntener, O. (2016). Amphibole-melt trace element partitioning of fractionating calc-alkaline magmas in the

lower crust: An experimental study. *Contributions to Mineralogy and Petrology, 171.* 10.1007/s00410-016-1278-0.

Ojakangas, R. W. (1968). Cretaceous sedimentation, Sacramento Valley, California. *Geological Society of America Bulletin, 79,* 973–1008.

Orme, D. A., & Surpless, K. D. (2019). The birth of a fore arc: The basal Great Valley Group, California, USA. *Geology, 47,* 757–761.

Padilla, A. J., Miller, C. F., Carley, T. L., Economos, R. C., Schmitt, A. K., Coble, M. A., et al. (2016). Elucidating the magmatic history of the Austurhorn silicic intrusive complex (southeast Iceland) using zircon elemental and isotopic geochemistry and geochronology. *Contributions to Mineralogy and Petrology, 171,* 69–90.

Paterson, S. R., & Ducea, M. N. (2015). Arc magmatic tempos: Gathering the evidence. *Elements, 11,* 91–98.

Pertermann, M., Hirschmann, M. M., Hametner, K., Gunther, D., & Schmidt, M. W. (2004). Experimental determination of trace element partitioning between garnet and silica-rich liquid during anhydrous partial melting of MORB-like eclogite. *Geochemistry, Geophysics, Geosystems, 5,* 23. 10.1029/2003GC000638.

Pickett, D. A., & Saleeby, J. B. (1994). Nd, Sr, and Pb isotopic characteristic of Cretaceous intrusive rocks from deep levels of the Sierra Nevada batholith, Tehachapi Mountains, California. *Contributions to Mineralogy and Petrology, 118,* 198–205.

Richter, K., & Charmichael, I. S. E. (1992). Hawaiites and related lavas in the Atenguillo graben, western Mexian Volcanic Belt. *Geological Society of America Bulletin, 104,* 1592–1607.

Saleeby, J., Ducea, M., & Clemens-Knott, D. (2003). Production and loss of high-density batholithic root, southern Sierra Nevada, California. *Tectonics, 22,* 1064–1088.

Sano, Y., Terada, K., & Fukuoka, T. (2002). High mass resolution ion micropobe analysis of rare earth elements in silicate glass, apatite and zircon: Lack of matrix dependency. *Chemical Geology, 184*(3), 217–230.

Schermer, E. R., Busby, C. J., & Mattinson, J. M. (2002). Paleogeographic and tectonic implications of Jurassic sedimentary and volcanic sequences in the central Mojave block, in Geologic Evolution of the Mojave Desert and Southwestern Basin and Range. *Geological Society of America Memoir, 195,* 93–115.

Shervais, J. W., Murchey, B. L., Kimbrough, D. L., Renne, P. R., & Hanan, B. (2005). Radioisotopic and biostratigraphic age relations in the Coast Range Ophiolite, northern California: Implications for the tectonic evolution of the Western Cordillera. *Geological Society of America Bulletin, 117*(5–6), 633–653.

Sisson, T. W. (1994). Hornblende-melt trace-element partitioning measured by ion microprobe. *Chemical Geology, 117,* 331–344.

Sisson, T. W., & Bronto, S. (1998). Evidence for pressure-release melting beneath magmatic arcs from basalt at Galunggung, Indonesia. *Nature, 319,* 883–886.

Sisson, T. W., Grove, T. L., & Coleman, D. S. (1996). Hornblende gabbro sill complex at Onion Valley, California, and a mining origin for the Sierra Nevada batholith. *Contributions to Mineralogy and Petrology, 126,* 81–108.

Strickland, A., Wooden, J. L., Mattinson, C. G., Ushikubo, T., Miller, D. M., & Valley, J. W. (2013). Proterozoic evolution of the Mojave crustal province as preserved in the Ivanpah Mountains, southeastern California. *Precambrian Research, 224,* 222–241.

Surpless, K. D., Clemens-Knott, D., Barth, A. P., & Gevedon, M. (2019). A survey of Sierra Nevada magmatism using Great Valley detrital zircon trace-element geochemistry: View from the fore arc. *Lithosphere, 11*(5), 603–619.

Tang, M., Lee, C-T. A., Chen, K., Erdman, M., Costin, G., & Jiang, H. (2019). Nb/Ta systematics in arc magma differentiation and the role of arclogites in continent formation. *Nature Communications,* (10), 235–241.

Tiepolo, M., Oberti, R., Zanetti, A., Vannucci, R., & Foley, S. (2007). Trace-element partitioning between amphibole and silicate melt. *Mineralogical Society of America, Reviews in Mineralogy and Petrology, 67,* 417–452.

Ulmer, P., Kaefi, R., & Muntener, O. (2018). Experimentally derived intermediate to silica-rich arc magmas by fractional crystallization at 1.0 GPa: An evaluation of phase relationships, compositions, liquid lines of descent and oxygen fugacity. *Journal of Petrology, 59,* 11–58.

Walker, J. D., Martin, M. S., & Glazner, A. F. (2002). Late Paleozoic to Mesozoic development of the Mojave Desert and environs, California, in Geologic Evolution of the Mojave Desert and Southwestern Basin and Range. *Geological Society of America Memoir, 195,* 1–18.

Wooden, J. L., Barth, A. P., & Jacobsen, C. E. (2018). Ce/Yb and Th/U fingerprinting of zircons: A way to distinguish Mesozoic magmatism in continental margin arcs from contemporaneous magmatism in the adjoining carton to the SW USA. *Geological Society of America Abstracts with Programs, 50*(6) n.. 10.1130/abs/2018AM-318252.

Wooden, J. L., & Miller, D. M. (1990). Chronologic and isotopic framework for Early Proterozoic crustal evolution in the eastern Mojave Desert region, SE California. *Journal of Geophysical Research, 95,* 133–220 p. 20146.